https://doi.org/10.5194/egusphere-2025-1398
Preprint. Discussion started: 11 April 2025

Quantitative parametrization of fracture networks in Digital Outcrop Models: an optimized workflow

Stefano Casiraghi[1], Gabriele Benedetti[1], Daniela Bertacchi[2], Silvia Mittempergher[1], Federico Agliardi[1], Bruno Monopoli[3], Fabio La Valle[4], Mattia Martinelli[4], Francesco Bigoni[4], Cristian Albertini[4], Andrea Bistacchi[1]

[1]Dipartimento di Scienze dell'Ambiente e della Terra, Università degli Studi di Milano-Bicocca, 20126 Italy
[2]Dipartimento di Matematica e Applicazioni, Università degli Studi di Milano-Bicocca, 20125, Italy
[3]LTS s.r.l., Treviso, 31020, Italy
[4]Eni S.p.A, Global Natural Resources

Correspondence to: Casiraghi Stefano (s.casiraghi21@campus.unimib.it)

Abstract. Mesoscale fractures, with lengths between meters and tens of meters, cannot be effectively characterized in the subsurface, due to limitations of borehole and geophysical datasets. On the other hand, large quantitative structural datasets can be collected on outcrops by combining direct observations and remote sensing (digital outcrop models - DOMs). These data can be used to constrain models of subsurface fracture networks with the outcrop analogue approach.

In this contribution we present a complete and rigorous workflow that leverages digital outcrop models with at least two perpendicular faces, in combination with various kinds of DOMs, to collect large multi-parameter datasets optimized to include all relevant statistical distributions.

Orientation data are collected with a semi-automatic procedure applied to point cloud DOM of the vertical side of the outcrop, resulting in 2D polygonal facets. Fracture sets are defined with a clustering procedure and different orientation distributions are fitted and if possible, tested with proper goodness-of-fit tests.

Fracture traces are digitized on textured surface or orthophoto DOMs. Topological parameters are calculated on the digitized fracture network on horizontal and vertical orthomosaics, also considering relationships with bedding. Trace length and height distributions are characterized with a robust innovative approach, accounting for the censoring bias with survival/reliability analysis. P_{21} (ratio between total fracture length and sampling area) is measured from traces digitized on the large horizontal outcrop, also allowing for the Representative Elementary Area (REA) to be assessed. Even if the height/length ratio cannot be measured on an outcrop by any means, we apply a realistic assumption and a regression test that avoids making completely theoretical assumptions not supported by data. We discuss the applicability of our workflow on a large top-quality fractured limestone outcrop in the Murge Plateau near Altamura (Puglia, Italy).

https://doi.org/10.5194/egusphere-2025-1398
Preprint. Discussion started: 11 April 2025

1 Introduction

Fracture networks are complex geological objects composed by all the fractures in a rock mass, were "fracture" is used here as a collective term for all the different types of discontinuities that affect rocks, including both primary features (e.g. bedding and foliation) and secondary discontinuities such as faults, shear fractures, joints, veins, stylolites and other dissolution features, deformation and compaction bands, dikes, etc. (Schultz, 2019). Fractures can be classified in sets, i.e. populations of cogenetic discontinuities related to the same deformation phases, kinematics (e.g. joint, normal fault), filling (e.g. quartz vein) and orientation, within statistical variability (Twiss and Moores, 2006; Davis et al., 2012).

Fractures exert a fundamental control on the mechanical and hydraulic properties of rock masses, and their relevance extends to multiple applications, including reservoirs of every kind of geofluid (e.g. Immenhauser et al., 2004; Pringle et al., 2006; Hodgetts, 2013; Wang et al., 2023), nuclear waste repositories (e.g. Follin et al., 2014; Hadgu et al., 2017), geothermal energy (e.g. Kosović et al., 2024), geo-hazard (e.g. Eberhardt et al., 2004; Agliardi et al., 2013; Riva et al., 2018), engineering geology (e.g. Franzosi et al., 2023a, b), seismic swarms migration (e.g. Cox, 2016), hydrothermal mineralization (e.g. Micklethwaite, 2009; Townend et al., 2017), and induced seismicity due to underground fluid injection (e.g. Karvounis and Wiemer, 2022). In recent years, the interest in fractured reservoirs has increased due to the growing number of projects related to decarbonization and the energy transition, such as CUS (Carbon Underground Sequestration; e.g. March et al., 2017, 2018), underground hydrogen storage (e.g. Wallace et al., 2021; Zamehrian and Sedaee, 2022), fractured aquifers and medium/high enthalpy geothermal fields (e.g. Genter et al., 2010), and underground energy storage (e.g. Menéndez et al., 2019). In all these applications, fracture patterns hold great importance as they influence the direction, magnitude, and heterogeneity of fluid flow, and the storage volume of reservoirs.

Parameter	Fracture network	Fracture set	Static/Dynamic
Number of sets	*		Static
Orientation		*	Static
Topology	*		Static
Size (length/height)		*	Static
H/L ratio		*	Static
Density/Intensity (1)	*	*	Static
Aperture		*	Dynamic
Spatial organization	*	*	Static
Representative Elementary Volume (2)	*	*	Static

Table 1 Summary of the fracture properties needed to quantitatively characterize a fracture network. (1) The P_{xx} system introduced by Dershowitz and Herda (1992) is generally used for density and intensity. (2) The representative

https://doi.org/10.5194/egusphere-2025-1398
Preprint. Discussion started: 11 April 2025

elementary volume (REV) can be different for each property and the overall REV of the fracture network can be seen as a combination of REVs for individual properties (e.g. Martinelli et al., 2020).

The quantitative characterization of fracture networks requires the determination of several geometrical and topological attributes of fractures and their statistical distributions (Table 1). Some of these attributes apply to the individual fracture set (e.g., orientation, length/height distribution) others to the whole fracture network (e.g., topology). Fracture properties can be static, meaning that they do not change in response to boundary stress field and fluid pressure variations (e.g., number and orientation of fracture sets), or dynamic, meaning that they can change due to variations of mechanical conditions, as for instance does fracture aperture when fluid pressure changes in response to injection of fluids in a reservoir or in the seismic cycle (Gleeson and Ingebritsen, 2012).

Several factors negatively impact our ability to quantify these parameters, both in the subsurface and in outcrops (e.g. Healy et al., 2017; Laubach et al., 2019; Martinelli et al., 2020):

1) Fractures in the subsurface (e.g. in reservoirs) cannot be characterized at the mesoscale (meters to tens of meters) using direct techniques. Borehole data (cores and image logs) only provide 1D, very local and sparse information (limited to 1D traces in a 3D volume), do not constrain the size of discontinuities, and are affected by important orientation biases (Baecher, 1983).
2) Geophysical methods can provide continuous 3D information, but with important limitations since (i) not always fractures are associated to a contrast in physical properties that can be imaged with geophysical techniques, and (ii) in any case the spatial resolution of these datasets is limited. For instance, in good quality industrial 3D seismics, fractures smaller than about 200-300m cannot be detected, and, in order to be directly observed, these fractures should be characterized by a displacement that results in a contrast of seismic impedance across the discontinuity. Summing up, only macro-scale faults can be reasonably imaged in seismics, and this induces a biased estimate of volumetric fracture metrics (e.g. Laubach et al., 2019).
3) At the outcrop scale four major biases must be taken into account (Baecher and Lanney, 1978): orientation bias, truncation bias, censoring bias and size bias. The orientation bias stems from the nature of the intersections between the fracture plane and the outcrop surface and to the choice of the sampling dimensionality (e.g., lines, areas or volumes). It influences the representativity of field measurements, and results in downsampling of certain fracture sets with respect to others. The truncation bias imposes a lower boundary to the measured fracture trace length, and it is defined by the smallest feature that is possible to detect. The censoring bias is due to the finite nature of outcrops since the full length of the longest fractures is limited by the outcrop size, and in any case the length of fractures ending outside of the outcrop is not known exactly. The size bias states that larger fractures (i.e. fracture surfaces with a larger area) have a greater probability to intersect the outcrop surface and to be sampled. To these major biases it is important to add that the morphological and weathering conditions of the outcrop strongly influence the calculation of parameters like topology, density and intensity.

https://doi.org/10.5194/egusphere-2025-1398
Preprint. Discussion started: 11 April 2025

4) A complete 3D description of the fracturing state is only possible in the lab at the centimetric to decametric scale, using non-destructive imaging techniques such as X-Ray Computer Tomography (Agliardi et al., 2014, 2017), which allow measuring volumetric parameters such as P_{33} (fracture porosity, i.e. fracture volume per unit volume), P_{32} (volumetric fracture intensity, i.e. fracture area per unit volume) and P_{30} (volumetric fracture density, i.e. fracture number per unit volume; Dershowitz and Herda, 1992).

The impossibility to directly map or image fractures in the subsurface suggested using continuum representations based on some form of upscaling or homogenization, such as the dual porosity model (Warren and Root, 1963). Alternatively, the Discrete Fracture Network (DFN) approach allows generating stochastic simulations where fractures are simplified as planar polygons in 3D or segments in 2D. Generating DFNs requires fracture parameters and a stopping criterion to end the simulation. Standard DFN software (e.g. Move – https://www.petex.com/pe-geology/move-suite/, Petrel – https://www.slb.com/products-and-services/delivering-digital-at-scale/software/petrel-subsurface-software/petrel, FracMan – https://www.wsp.com/en-gl/services/fracman, DFNworks – https://dfnworks.lanl.gov/) are based on a Poisson point process that generates fractures with a random spatial distribution. The geometrical properties of each fracture are drawn from parametric length and orientation distributions, and fracture height is generally controlled by a fixed height/length ratio. The simulator generates fractures until a target fracture intensity P_{32} (Dershowitz and Herda, 1992) is reached in the simulation volume. Connectivity or any other form of spatial organization cannot be taken into account in these models due to limitations of the Poisson distribution, that is specifically based on the assumption of spatial independence between fractures (e.g. Davis, 2002). Modern approaches have been developed in the last years to try and solve this fundamental limitation, for instance controlling clustering of fractures by means of the Ripley's K function (Shakiba et al., 2024), or including attractive vs. repulsive spatial and directional processes controlled by statistical and/or pseudo-mechanical parametrizations (Bonneau et al., 2013; Davy et al., 2013; Bonneau et al., 2016), but a satisfactory solution has yet to be found, especially in 3D. Sometimes also "deterministic" DFNs are used, but the possibility of creating such models is limited to structures that can be imaged in 3D seismics, i.e. meso-scale faults larger than some hundred meters and characterized by an offset that results in a contrast in seismic impedance.

Due to the beforementioned limitations in subsurface datasets, input properties for generating stochastic DFNs are often obtained from representative analogues exposed in outcrops that can be studied in detail, compensating for the information gap at the reservoir scale. The outcrop analogue approach assumes that the detailed information gathered at selected, high-quality rock outcrops can be considered representative of the fracture network properties of deep rock masses that underwent the same geological history (Bertrand et al., 2015; Bistacchi et al., 2015; Jacquemyn et al., 2015; Martinelli et al., 2020).

This approach relies on the availability of robust datasets to characterize statistical distributions of the fracture network. In this regard, the traditional direct geological and structural field survey is as unavoidable as it is limiting, in the sense that parameters such as kinematics, roughness, relative chronology and mineralization/filling of structures can only be gathered during fieldwork (e.g. Hancock, 1985), but on the other hand limited accessibility and logistical limitations prevent the collection of extensive geometrical datasets with traditional techniques (e.g. McCaffrey et al., 2005). To solve this problem,

https://doi.org/10.5194/egusphere-2025-1398
Preprint. Discussion started: 11 April 2025

Digital Outcrop Models (DOMs) - high-resolution 3D photorealistic representations of natural outcrops (Bellian et al., 2005; Bistacchi et al., 2022b) have been successfully employed to collect large quantitative structural datasets, overcoming the limitations of classical survey techniques (Sturzenegger and Stead, 2009; Gigli and Casagli, 2011; Sturzenegger et al., 2011; Riquelme et al., 2014, 2015; Bistacchi et al., 2020; Martinelli et al., 2020; Bistacchi et al., 2022a; Storti et al., 2022).

Depending on the outcrop morphological expression, data can be collected from DOMs using either facets - 2D planes interpolated on the DOM, or traces - polylines that are usually digitized in a GIS environment, but sometimes also on a 3D DOM (Bistacchi et al., 2022b). These two types of data carry different but complementary information; however, the methodologies developed in previous contributions by different authors are often based on only one of these kind of data, limiting the number of parameters that can be obtained (Ortega et al., 2006; Boro et al., 2014; Martinelli et al., 2020; Smeraglia et al., 2021).

In this paper we present a workflow that combines new and existing methodologies to quantitatively characterize all the parameters of a fracture network, with a particular focus on obtaining robust statistical distributions to be used as input in stochastic DFN models. The analysis is based on both traditional direct field observations and photogrammetric DOM analysis. The integrated workflow is aimed at maximizing the structural information that can be obtained from different types of DOMs, including orientation distributions, topological relationships, length and height distributions and fracture intensity. Some of these parameters (i.e. topology) are not direct inputs to DFN models, yet they represent a fundamental control on the quality of the generated model itself.

The workflow, rooted in a rigorous statistical background, attempts at minimizing the assumptions made at every step, for example during the choice of the orientation distribution, or the length and height distribution. The methodologies proposed to estimate each parameter can be applied independently, subject to the type and quality of the outcrop. The complete workflow (Figure 1), combining both facet and trace data, includes two separate processing pipelines: (i) semi-automated fracture orientation analysis carried out on point cloud DOMs (Sect.4.4); and (ii) fracture trace analysis carried out on orthomosaics, allowing to measure topological relationships, length and/or height distributions, P_{21}, and to estimate (subject to assumptions) the H/L ratio distribution (Sect. 5 to 8). The two pipelines are integrated to achieve a complete 3D parametrization of the fracture network (Sect. 9 and following).

We tested our workflow at an abandoned quarry of the Altamura Limestone Fm. (Puglia, Italy), where both a horizontal pavement and vertical walls provide the opportunity to fully characterize the fracture network in 3D.

https://doi.org/10.5194/egusphere-2025-1398
Preprint. Discussion started: 11 April 2025

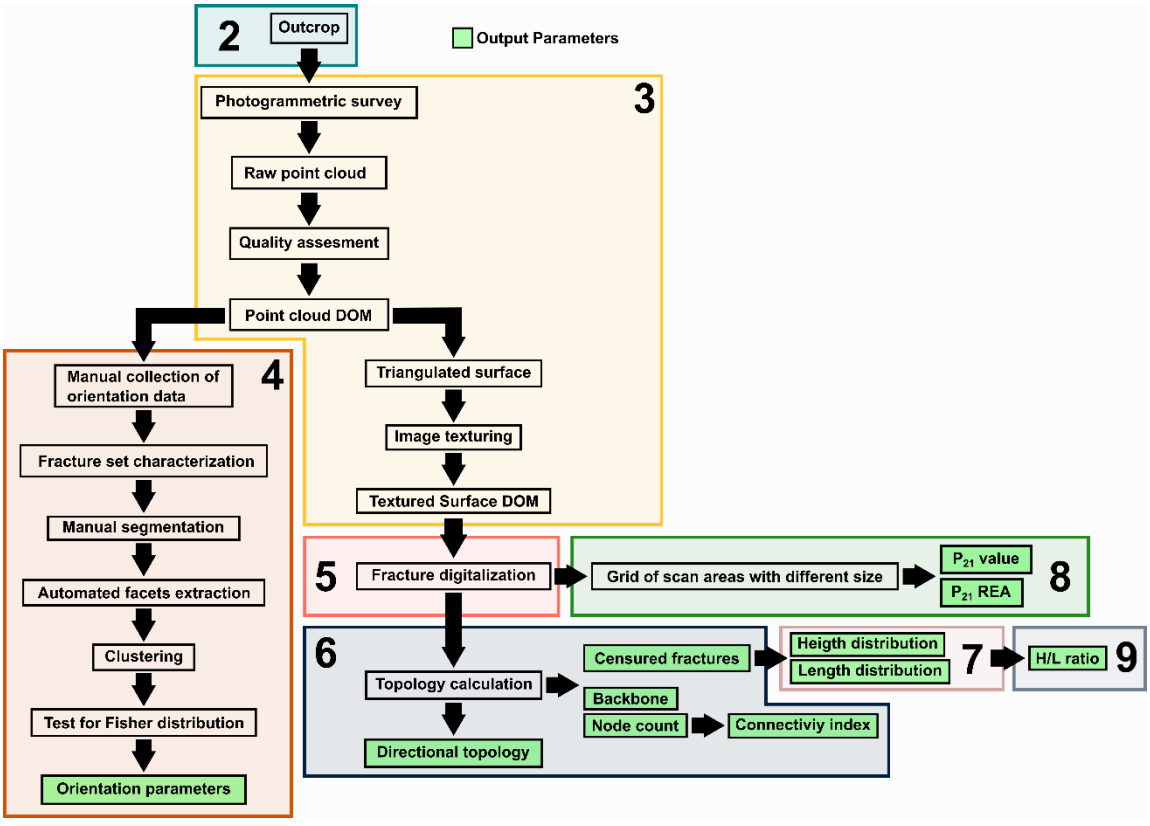

Figure 1 Flow chart of the presented workflow. Numbered boxes define the sections of this contribution in which the respective steps of the workflow are addressed.

2 Selecting an outcrop: the Altamura Limestone at Pontrelli quarry

Outcrops for quantitative fracture survey needs to be carefully selected, in order to satisfy some requirements: a) representativity of the structural and lithological properties of the larger rock volume of interest (e.g. some formation, a fold limb, etc.); b) size large enough to account for the scale of structures to be investigated; c) continuous unimpeded exposure; d) optimal orientation with respect to the main fracture sets, to minimize orientation biases (Terzaghi, 1965; Zhang et al., 2002). In this context, it is important to select outcrops that present at least two exposed perpendicular sides (e.g., a vertical cliff and an exposed pavements), natural or artificial (e.g., quarry site), for a full 3D characterization of the fracture network metrics.

Here we consider fractured limestone outcrops in the Murge Plateau near Altamura (Puglia, Italy), in the forebulge of the outer Apulian platform, in front of the southern part of the Southern Apennines fold and thrust belt (Panza et al., 2019). The abandoned Pontrelli quarry provides 18.000 m^2 of horizontal pavement and vertical walls with a cumulative width of up to 500m and up to 6m in height, where fractures are beautifully exposed thanks to the careful maintenance of the site (Figure 2A, B, C) that is carried out because of thousands of dinosaur footprints that were discovered by Nicosia et al. (1999). The

https://doi.org/10.5194/egusphere-2025-1398
Preprint. Discussion started: 11 April 2025

outcrop, well known and described in scientific literature (Panza et al., 2015, 2016, 2019) has been recognized as a suitable analogue for reservoirs in related areas (Zambrano et al., 2016).

The quarry is carved into the shallow marine intertidal limestones of the Calcare di Altamura Formation. Limestones are well-stratified light-brown mudstones, with wackestone-packstone layers at the bottom of the beds and sometimes algal laminites in the upper parts. Strata are 20 – 60 cm thick and are organized in thickening upward cycles, some meters thick, bounded at the top by major surfaces of subaerial exposure. Bed interfaces often consist of stylolites having teeth both perpendicular to the folded bedding and tangential (slickolites). The outcrop shows 3 different fracture sets and a set of "major" structures, that are actually major at the outcrop scale, but negligeable at the regional scale (Figure 2B). Set 1 is the most persistent, it is NW-SE striking and, based on abutting relationships, predates all the other sets (Table 2). It presents both joints and meso-faults with a vertical displacement up to a few cm. Set 2 is also striking NW-SE on average, but with a wider scatter, and it also includes both joints and strike-slip meso-faults. However, structures belonging to Set 2 always abut on those belonging to Set 1, showing that Set 2 is distinctly younger (Table 2). Set 3 is NE-SW striking and includes fractures that abut on those belonging to both Set 1 and 2. The trace of these fractures, that are limited by older structures, are relatively short, but are responsible of most of the connectivity of the network (Table 2).

Even though this outcrop is top-quality in terms of fracture parameterization, due to the areal extension, cleanliness of the pavement, and the association between horizontal and vertical outcrops, some problems must be still evaluated.

The pavement (Figure 1A, B) presents some no data zones – where no data can be collected at all, due to debris patches or the presence of strong concentrations of non-natural features produced by quarrying activities. Other zones distributed across the pavement are partially affected by non-natural, quarrying-related fractures, but with a careful analysis it is still possible to detect Set 1, while Set 2 and especially Set 3, being characterized by smaller fractures, are drowned by artificial fractures.

Regarding the quarry walls, here we present data on the NW part (Figure 2C), that is less disturbed by quarrying activities and favourably oriented with respect to Set 1 and 2, while Set 3 is sub-parallel to the wall. The wall is around 6m tall, and according to the stratigraphic analysis proposed by Panza et al., (2016), includes a bed package developed above the quarry pavement, which is one major subaerial exposure surface, while other prominent subaerial exposure surfaces are not detected inside the wall.

https://doi.org/10.5194/egusphere-2025-1398
Preprint. Discussion started: 11 April 2025

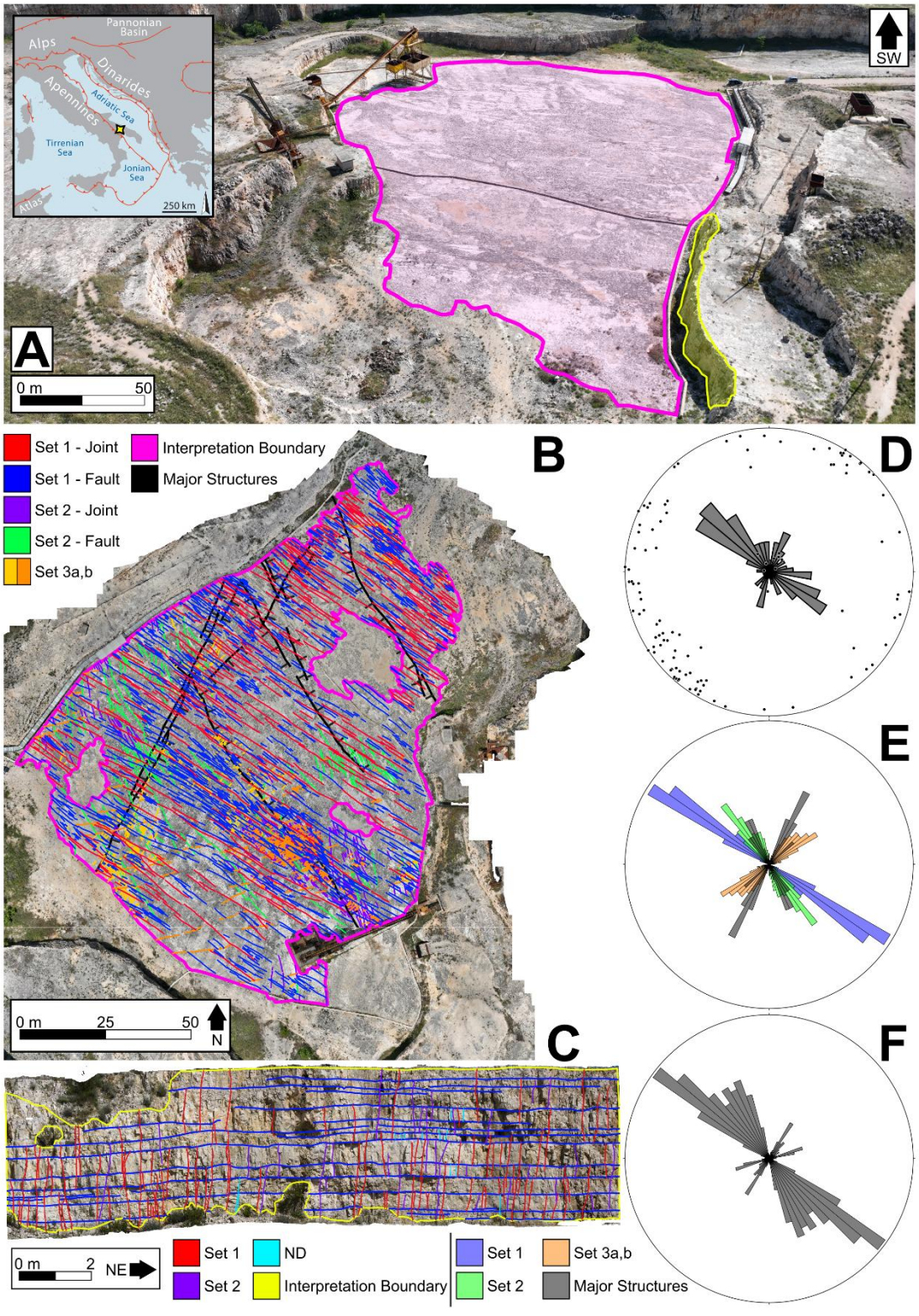

https://doi.org/10.5194/egusphere-2025-1398
Preprint. Discussion started: 11 April 2025

Figure 2 (A) Aerial view of the Pontrelli quarry, Altamura, Italy. In pink the quarry pavement is highlighted, while the analysed quarry wall is highlighted in green. (B) Orthomosaic of the quarry pavement, with digitized fractures and interpretation boundary. (C) Orthomosaic of the interpreted vertical wall, with digitized fractures and interpretation boundary. (D) Field data collected along the quarry walls. (E) Rose diagram of orientation data collected from fracture traces on the orthophoto of the pavement (B). (F) Rose diagram of orientation data collected from fracture facets on the digital outcrop shown in (C).

Fracture set	Structures & kinematics	Average strike	Relative chronology
Set 1	Joints and meso-faults	NW-SE	Abutted by Set 2 & 3
Set 2	Joints and meso-faults	NW-SE	Joints abut on Set 1 & abutted by Set 3. Faults crosscut Set 1 & abutted by Set 3.
Set 3	Joints	SW-NE	Abut on Set 1 and 2

Table 2 Summary of fracture sets characteristics at the Pontrelli quarry.

3 Digital Outcrop Model reconstruction and pre-processing

Once the best exposures have been selected, we must also take care of collecting the best input data in order to create a high-quality DOM, that will greatly facilitate the workflow downstream. This topic was covered in details by Bistacchi et al. (2022b) and here we just summarize the main requirements in the next paragraphs, always considering the Cava Pontrelli case study.

3.1 Photogrammetric acquisition

Horizontal pavement DOMs have been acquired with a DJI Mavic 3E drone flown with an autonomous flight application (DJI Fly app). The photos were shot perpendicular to the outcrop, with a 70% overlap, both between photos pertaining to a single strip and between adjacent strips. As discussed in Bistacchi et al. (2022b), flights at different altitudes were collected to avoid large-scale distortion in the photogrammetric model, and the minimum altitude of 8m allowed collecting images with a ground resolution of 4 mm/pixel. Georeferencing of these DOMs is based on GPS data collected by the drone and recorded in EXIF data of each photo.

Vertical cliff DOMs have been collected with a Nikon Z7 full-frame mirrorless camera mounted on a tripod with a graduated head, adopting a multiple fan scheme (Bistacchi et al., 2022b), in which every shooting station is evenly spaced by 10° of interstation vision angle, measured targeting a certain point on the outcrop and moving parallel to the outcrop by a distance corresponding to 10°. From each camera locations several photos were shot with a fan pattern, trying to cover the whole outcrop and using different focal lengths, and some shooting stations were collected from a larger distance. This shooting scheme allows (i) avoiding large-scale distortion in the photogrammetric model and (ii) results in an optimal reconstruction

https://doi.org/10.5194/egusphere-2025-1398
Preprint. Discussion started: 11 April 2025

of rough outcrop faces, characterized by facets that form a high angle with respect to the main viewpoint. Noteworthy, this kind of survey could be also carried out with a drone, flying and shooting manually, replicating the ground-based multiple fan scheme, but only high-end cinema-grade drones have cameras that can come close to the quality of a high-end full frame DLSR or mirrorless camera, with significantly higher costs, hence where possible we prefer to use the ground-based technique.

Georeferencing of the terrestrial surveys was simply performed by marking on the outcrop the location of the mirrorless camera shooting stations before carrying out the drone survey. These points were then retrieved from the drone dataset with an accuracy of better than 4 mm (allowed by the very high resolution) and used to co-locate the terrestrial dataset in an accurate and perfectly consistent way.

3.2 Point cloud DOM and Textured surface DOM

Regardless of the technique used to acquire the data, DOMs can be rendered, depending on the outcrop morphology and the scope of the work, as point cloud DOMs (PC-DOMs) or textured surface DOMs (TS-DOMs) (Bistacchi et al., 2022b). PC-DOMs, as the name suggests, are dense sets of points, where each point is characterized by XYZ coordinates and an RGB value, and they are the main output of SFM/MVS photogrammetric reconstructions or laser scanning acquisitions. PC-DOMs are particularly suitable to carry on structural interpretations, using specific tools (Thiele et al., 2018), on outcrops where fractures appear as facets of different size and orientation (as in Figure 3). TS-DOMs are derived from PC-DOMs by generating a polygonal mesh from the point cloud and texturing images onto its surface (Tavani et al., 2014; Bistacchi et al., 2015). In this case the geological and structural interpretation can be carried out in 3D or, as we do in this contribution, with a standard 2D Geographical Information System (GIS) environment (e.g., QGIS).

3.3 Quality of the photogrammetric model

Defining an absolute quality criterion for a point cloud obtained from a photogrammetric survey is not easy, as different kinds of applications have different requirements. In our application scenario, absolute precision is of lesser priority with respect to the relative accuracy within a local reference frame. This can be evaluated in early stages of the photogrammetric processing considering the image reprojection error, measured in pixels, as it directly impacts the relative accuracy of the photogrammetric model as a fraction of its ground resolution (expressed in mm/pixel).

A fundamental requirement in a DOM aimed at structural analysis is that it must be completely free from artifacts (doubled surfaces, distortion, doming), and that noise (isolated points outside the outcrop surface) should be as low as possible. A typical artifact resulting from a low-quality acquisition scheme, that does not include fans or photos collected at variable altitude as discussed above, is the presence of doubled “surfaces”, consisting in layers of duplicated points that do not define univocally the outcrop surface. Bistacchi et al., 2022b suggested that the best solution is to use a high-quality acquisition scheme, since *a posteriori* solutions do not work or are hugely time-consuming.

https://doi.org/10.5194/egusphere-2025-1398
Preprint. Discussion started: 11 April 2025

We believe that the most important parameter for applications in structural geology is surface density. By defining a kernel - a sphere of radius R moving in such a way as to being cantered on each point - the point surface density SD can be calculated as the ratio between the number N of points falling in the kernel and the area πR^2 of the largest circle inscribed in the sphere with radius R:

$$SD = \frac{N}{\pi R^2} \quad (1)$$

As an example, in Figure 3, two PC-DOMs of the same vertical outcrop are compared, collected in two different ways to obtain a different SD. The PC-DOM in Figure 3D is reconstructed from more than 400 photos collected as discussed above (terrestrial survey with fans scheme, with high end Nikon Z7 mirrorless). On the other hand, the PC-DOM in Figure 3C is collected with a smaller dataset (150 photos) collected with the lower quality camera of a small commercial drone (DJI Mini 3 Pro). The mean *SD* of the PC-DOM shown in Figure 3D is two orders of magnitude higher than the PC-DOM of Figure 3C (298826 vs. 5249 points/m^{-2}), resulting in a much sharper point cloud, from which it is possible to extract more easily, much more structural information.

In conclusion a good PC-DOM must be free of artifacts, have low noise, and have a very high SD on all surfaces of interest, including facets that form a high angle with the outcrop mean plane, which can be properly imaged only if a multiple fans scheme is used.

https://doi.org/10.5194/egusphere-2025-1398
Preprint. Discussion started: 11 April 2025

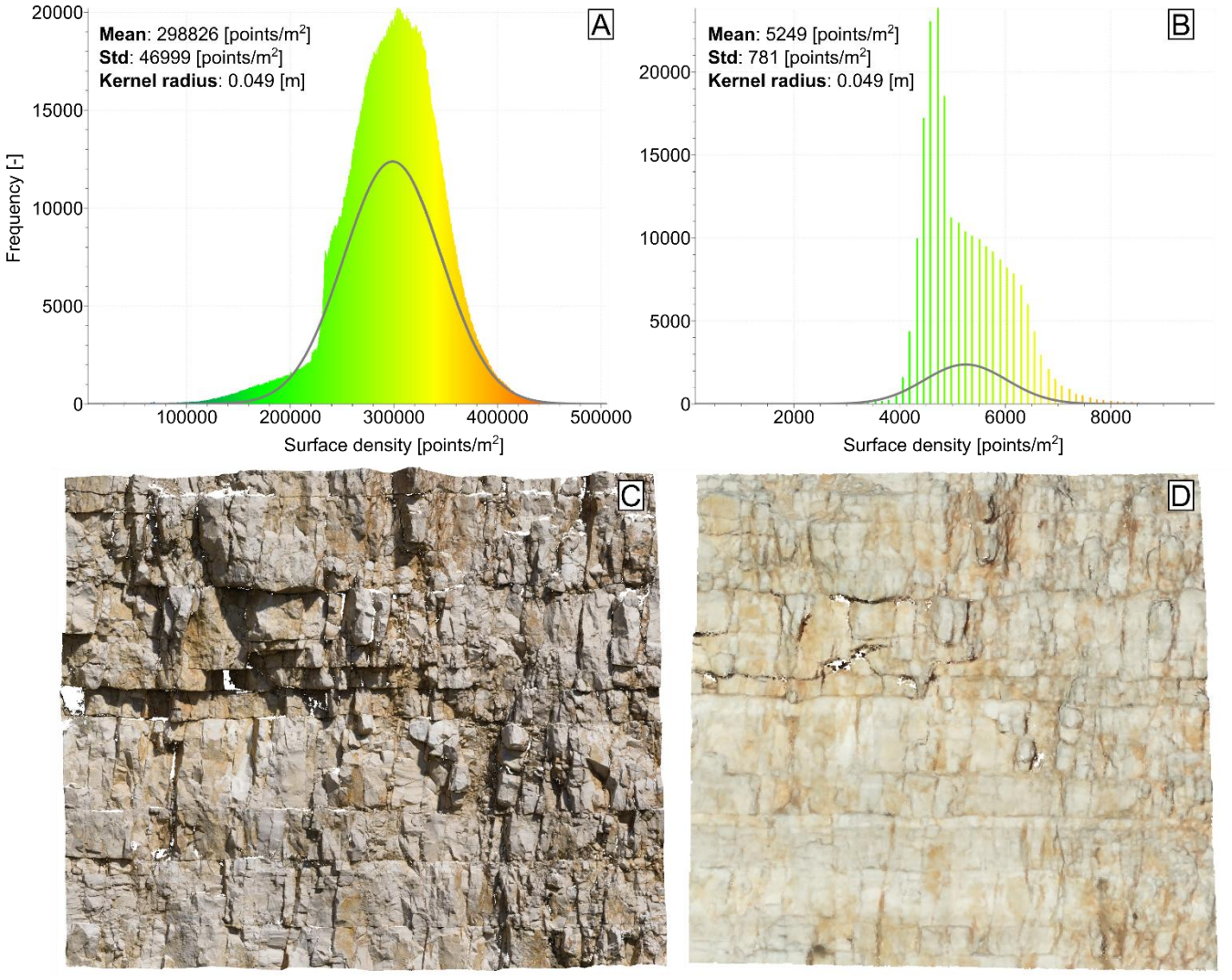

Figure 3 Comparison between two different PC-DOMs of the same vertical outcrop. (A) and (B) frequency distribution of the *SD* measured with a kernel of 0.049m. The parameters are obtained by fitting a Gaussian model. (C) PC-DOM reconstructed from photos collected with a high-resolution full-frame mirrorless camera. (D) PC-DOM reconstructed from photos collected with a commercial drone and a simplified acquisition scheme. Point size has been magnified five times, for visualization reasons.

4 PC-DOM: semi-automated analysis of fracture orientation

The goals of orientation analysis are to measure the attitude of each fracture facet that can be mapped on the DOM and to classify it within a fracture set (i.e. a statistically defined fracture cluster), amongst those identified in the preliminary field survey, or emerging from the clustering analysis (Section 4.3), and finally to obtain robust orientation statistics for each fracture set.

https://doi.org/10.5194/egusphere-2025-1398
Preprint. Discussion started: 11 April 2025

Fractures in PC-DOMs are mainly represented by point patches that are the morphological expression, on the outcrop surface, of fracture surfaces, exposed due to natural (e.g. erosion or rockfall) or anthropic (e.g. excavation) events. Here we propose a semi-automatic workflow to map these patches, based on a first step of manual mapping of a subset of fracture planes on the PC-DOM. This allows selecting different sets of structures, characterizing their orientation statistics, and assigning them to sets defined in the field. Based on dip and dip direction ranges, the PC-DOM is manually segmented into as many parts as the number of recognized fracture sets. The automatic step consists in the automatic interpolation of 2D planar features from the segmented point cloud, eventually allowing to greatly increase the number of facets included in the analysis, with important benefits for the statistical analysis (Figure 5).

Our workflow can be carried out in CloudCompare (https://www.danielgm.net/cc/), the most used open-source software for point cloud processing (Dewez et al., 2016; Thiele et al., 2018) or in PZero, a new 3D geomodelling application where we are also developing new tools for DOM analysis (github.com/gecos-lab/PZero).

4.1 Orientation parameters for fracture sets

Orientation data are usually recorded in geology using polar coordinates, either as dip and dip direction (dip azimuth) or dip and strike for planar features, or as plunge and trend for axes. In general, any orientation can be represented as a unit vector within a three-dimensional spatial framework (e.g. Mardia and Jupp, 2000), and polar coordinates can be converted into director cosines in a dextral cartesian reference with:

$$L = \sin(dir)\cos(dip) \quad (2)$$

$$M = \cos(dir)\cos(dip) \quad (3)$$

$$N = -\sin(dip) \quad (4)$$

where L is the component in direction East, M is directed towards the North, and N is directed upwards (Borradaile, 2003).

The unit normal vector ($\vec{v} = L, M, N$) is calculated on every point of the point cloud by fitting a plane to the points that fall within a sphere of specified radius, cantered at the point itself. The larger the radius the smoother the normal vectors will result, with the drawback of longer computational times.

With a few exceptions (e.g. bedding with polarity, flow directions), the orientation of geological structures and particularly of deformational features like fractures shows a symmetry where the sense does not bear any geological meaning. In mathematical terms this means that two vectors $\vec{v}$ and $-\vec{v}$ are equivalent in this kind of analysis. This means that different conventions can be used for the sense of normal vectors, i.e. the geological convention where normal vectors always point downwards or the photogrammetric convention where they point out of the outcrop.

https://doi.org/10.5194/egusphere-2025-1398
Preprint. Discussion started: 11 April 2025

4.2 Manual orientation mapping

The first step of the workflow is carried out by manually mapping facets, and particularly their attitude, in the PC-DOM with the Compass plugin in CloudCompare (Thiele et al., 2018) or with the facet mapping tool in PZero. These tools behave in the same way and mimic the process of manually collecting attitude data in the field with a geologist compass-clinometer. The fundamental goal of this step of the workflow is to sample each set to define its dip and dip direction range, that will be used in the manual segmentation step. Therefore, we suggest carrying out the mapping with an initial random sampling and then avoiding oversampling the most represented sets (that are generally those favoured by the outcrop orientation bias).

Dip and dip direction values are obtained by fitting a local plane on points selected with a spherical kernel. The kernel radius is defined on-the-fly during mapping by the user, based on the dimension of the fracture plane. A too small kernel will result in measurements affected by the roughness of the fracture plane, while a too big kernel will include points pertaining to other planes, biasing the orientation value. Orientation data collected in this way are plotted in stereoplots and compared with data collected in the field (Figure 2D), in order to assess whether all field-defined sets are also represented in the digital dataset.

4.3 K-medoid clustering

The precise identification of fracture clusters is fundamental in the following automated segmentation step, where each fracture set corresponds to a cluster of orientation data that can be uniquely defined with a measure of location – a series of measures to locate the fracture cluster in the parameter space (e.g., mean L, M, N), and a measure of concentration or dispersion (Borradaile, 2003). Clustering analysis provides a quantitative answer to both the number of clusters the dataset is composed of, and the parameters of each cluster, given an assumption on the type of distribution.

We apply the K-medoid method to a dataset represented by a table, with n rows corresponding to individual orientation data and three columns corresponding to the three director cosines. K-medoids is a partitional method (Kaufman and Rousseeuw, 1987) aimed at classifying the data into k_m groups, where k_m is the number of fracture set defined in the field, eventually adjusted by the visual inspection of the plotted data . Each group must contain at least one object, and each object must belong to only one group. Partitional methods try to find a suitable partition by separating objects close to each other from objects far away from each other, and how the proximity between objects is calculated determines the specificity of the method. Considering K-medoids in a 3D parameter space (L, M, N), the location parameter is defined by a medoid, i.e. the point belonging to the cluster that minimizes the average distance in the 3-dimensional space between all the other data belonging to the cluster and the medoid itself (Kaufman and Rousseeuw, 1987, 2005). K-medoids therefore measure distance in an isotropic way in the 3-dimensional space of the dataset. When compared to the more popular K-means approach, K-medoids are more robust and less affected by outliers (Kaufman and Rousseeuw, 1987).

One of the problems that arises with K-medoids and other similar partitional methods lies in the definition of the approach itself, as the number k_m of cluster is imposed by the user, and this can lead to an underestimation or overestimation of the real number of clusters (Kaufman and Rousseeuw, 2005). However, in our application this is not a problem, since the

https://doi.org/10.5194/egusphere-2025-1398
Preprint. Discussion started: 11 April 2025

number of fracture sets is iteratively defined starting from an initial guess defined in the field and the clustering algorithm is applied as a validation of that hypothesis, eventually adjusting the number of sets to account for clusters that only surfaced during the statistical analysis.

A second drawback is that in the standard implementation the initial guess for the medoids is chosen randomly, and when different fracture sets show a partial superposition, the clustering algorithm could yield inconsistent and unreliable results. To address this issue, the initial guess can be defined by the interpreter by manually positioning the initial guess for the medoid.

Finally, to avoid the sense ambiguity of orientation unit vectors discussed above, particularly critical for clusters of sub-horizontal vectors that can be mirrored across the stereoplot equator, we have developed a solution based on mirroring all input data. For each input vector $\vec{v_i}$ we create another vector $-\vec{v_i}$ with parallel direction and opposite sense (i.e. pointing in the upper hemisphere (Figure 4). Then we perform the K-medoids clustering on this duplicated dataset, extracting $2k_m$ clusters both in the upper and lower hemisphere. Given the symmetry imposed by duplicating the data with mirroring, also the resulting $2k_m$ medoids will be symmetrical, with each medoid in the lower hemisphere having a perfectly symmetrical pair in the upper hemisphere and vice versa, then to conclude the analysis we extract just the k_m clusters with the medoid pointing downwards, in the lower hemisphere (Figure 4).

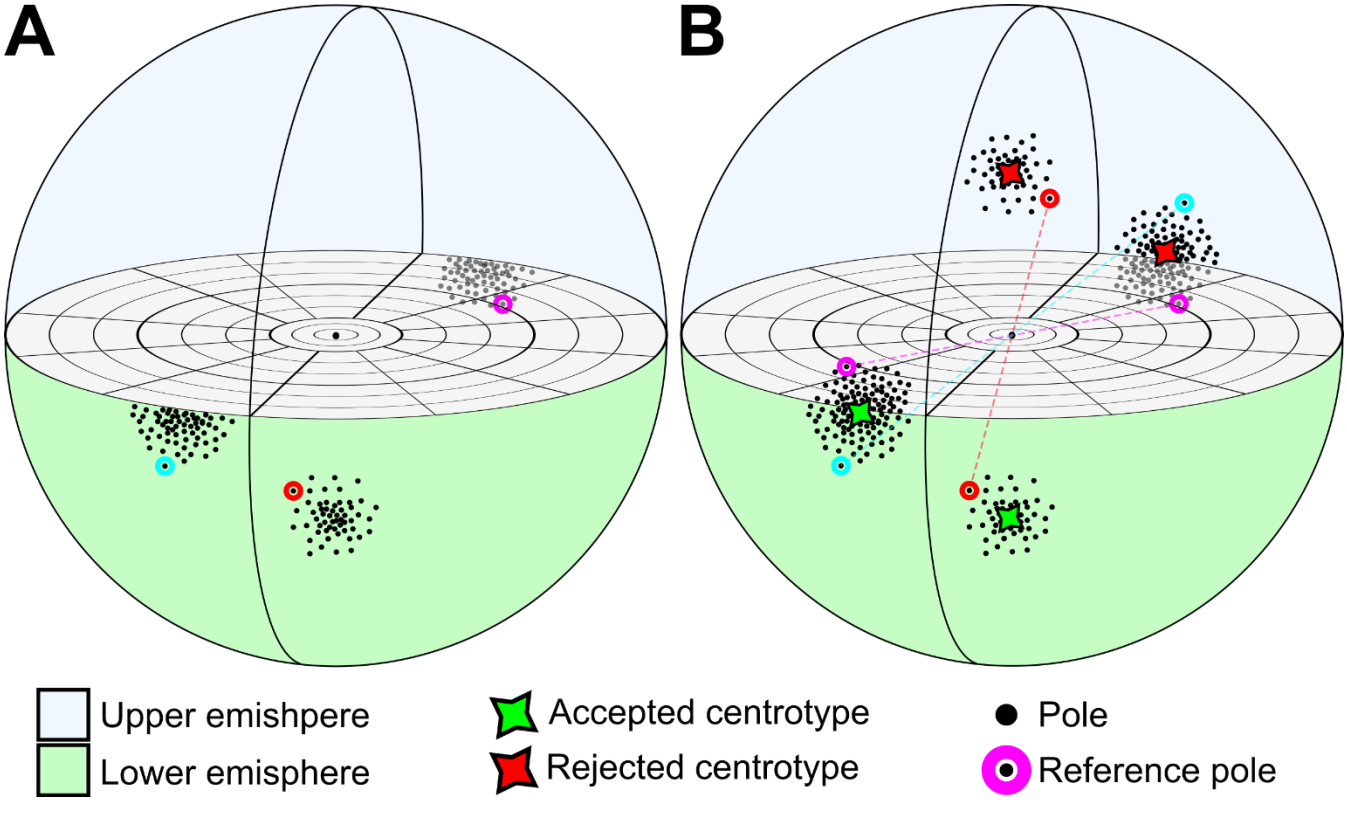

https://doi.org/10.5194/egusphere-2025-1398
Preprint. Discussion started: 11 April 2025

Figure 4 (A) 3D stereoplot of two hypothetical fracture set collected on the field. Light blue set and magenta set are the same set but recognized as two different sets, due to the geological sign convention. (B) Every set is doubled and mirrored with respect to the center of the sphere (B). The clustering algorithm is applied on double the number of the set and only the centrotypes that follow the geological sign convention are kept (B).

4.4 Manual segmentation of PC-DOM and semi-automatic planar feature extraction

Based on orientation statistics and K-medoids clustering, it is now possible to segment the whole point cloud into subsets with normal unit vectors falling within the statistical variability of different fracture sets.

The subsets are composed of isolated clusters of points, with the same orientation, each representing a portion of a separated fracture plane. This greatly improves the automatic extraction of 2D polygonal features during the following steps because every patch of points is isolated from the others, nullifying the risk of merging adjacent clusters into one bigger 2D polygon and avoiding the possibility of generating planes with an averaged orientation between two different point clusters, pertaining to two different fracture sets with different orientations. Another advantage of the manual segmentation is that it is possible to specifically calibrate the algorithm for each fracture set.

The segmented point cloud subsets are then fed to the CloudCompare FACETS plugin (Dewez et al., 2016), and specifically to its fast-marching algorithm (Sethian, 1999), to interpolate a planar polygonal feature per every point patch that matches the calibrated algorithm parameters. In this context, manual mapping and orientation analysis act as a calibration step in preparation for the final automatic extraction of planar features, that is greatly simplified and results in very clean results thanks to the segmentation step, that for instance avoids generating spurious facets.

https://doi.org/10.5194/egusphere-2025-1398
Preprint. Discussion started: 11 April 2025

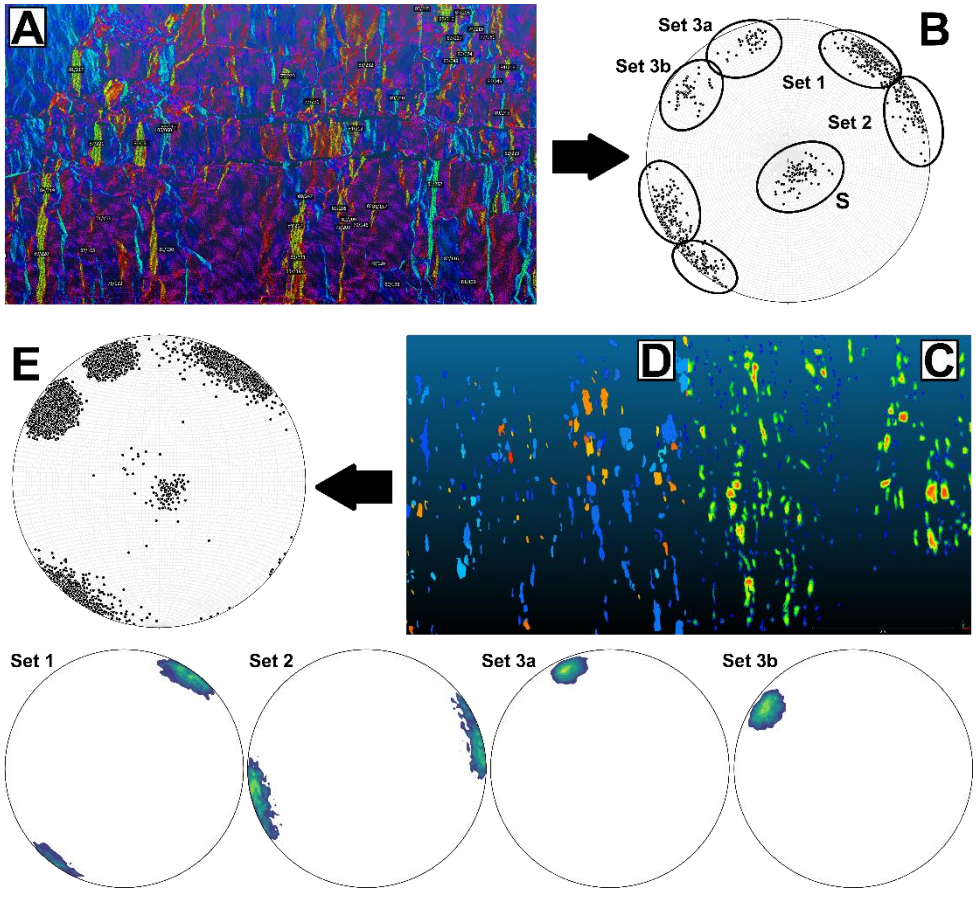

Figure 5 Scheme of the semi-automatic workflow presented in Section 4. Point cloud colored based on dip direction with a HSV colour scale. (A) Manual data collection on PC-DOM. (B) Manually collected orientation data during the preliminary orientation analysis. (C) Manual segmentation of the PC-DOM. (D) automatic feature detection with FACETS plugin. (E) Final result of the semi-automatic extraction workflow. Each fracture set is individually shown with contour lines.

Fast marching algorithms are a class of methods developed to track propagating interfaces into a bi-dimensional or three-dimensional space (Sethian, 1999). In the FACETS plugin (Dewez et al., 2016), the fast-marching algorithm is employed to create polygonal planar surfaces interpolating subsets of the point cloud. The algorithm is based on four parameters that need to be calibrated for optimal results. In particular:

- *Octree level* defines the level of systematic recursive subdivision of the point cloud three-dimensional space, defined by its bounding box, in this case, a cube. Every level involves subdividing the box into 8 sub-cubes, that allow optimizing the definition of the smallest feature we want to detect (i.e. the scale of analysis), with the computational time increasing with the level. No specific strategy exists to calibrate the octree level. As a starting guess we should chose a value that results in cubes with a dimension comparable to the smaller fracture facet we want to detect. From this value, it is

https://doi.org/10.5194/egusphere-2025-1398
Preprint. Discussion started: 11 April 2025

possible to decrease or increase the octree level by one level, visually checking the results. In our experience, increasing too much the octree level does not increase the quality of the analysis but will result in an over-segmentation of the facets and possibly in a noise increasing.

- *Maximum distance* defines a generalization criterion to merge adjacent features. For instance, if maximum distance is set at 68%, at least 68% of the points associated to a facet must have a distance to the facet mean plane that is lower than the standard deviation of the distances from the mean plane fitted from the points defining the facet. In geological terms, this parameter controls the maximum roughness accepted for a plane to be fitted. The maximum distance parameter can be calculated by manually isolating a certain patch of points, representing a fracture plane. The distance from the mean plane of every point can be manually calculated by fitting a mean plane to the point patch. The result is given in the form of a scalar field associated to the point cloud. The mean distance is calculated by fitting a Gaussian model to the frequency histogram of the previously calculated distances.
- *Minimum points per facet* defines the minimum number of points needed to define a facet. The higher the octree level, the smaller this parameter should be, as the dimension of the smallest feature detected decreases and so the related number of points. This parameter can be considered a threshold between what we consider as noise, and what we consider as a proper feature. The minimum points per facet parameter must be tuned according to the average surface density SD of the PC-DOM. The higher the surface density the higher will be number of points in the smaller element produced by the octree subdivision, therefore the higher this parameter can be set.
- *Maximum edge length* is related to the length of the boundary of the facet. Small values of this parameter impose concave and compact boundaries, while larger values allow for elongated and/or convex boundaries. There is no general rule for the calculation of this parameter, which must be empirically calibrated on a case-by-case basis.

Calibrating all these parameters on the whole point cloud is taxing in terms of computational time, therefore we suggest selecting at least 30 representative facets (Fisher, 1992), in terms of dimension and roughness, for every fracture set, calibrating the algorithm parameters on these facets, and then use this calibration to process the whole PC-DOM. When working on a single facet, the octree level must be set to 0, as an isolated facet is considered as a point cloud on its own (Figure 6).

The result of the feature extraction algorithm is a set of 2D polygonal facets resulting from the interpolation of point patches that met the criteria defined in the calibration, from which orientation parameters will be obtained (Figure 7E).

It is important to remember that facets can be interpolated only on fully exposed planar structures, therefore they represent only the part of the fracture plane that shows a morphological expression. Moreover, based on the calibrated parameters there is the possibility that the interpolation of an exposed surface will result in a combination of facets, and not a single one. All of this to say that data like faces height and surface extension can be useful but should be handled with care if trying to obtain volumetric parameters (P_{30} or P_{32}) or height distributions.

https://doi.org/10.5194/egusphere-2025-1398
Preprint. Discussion started: 11 April 2025

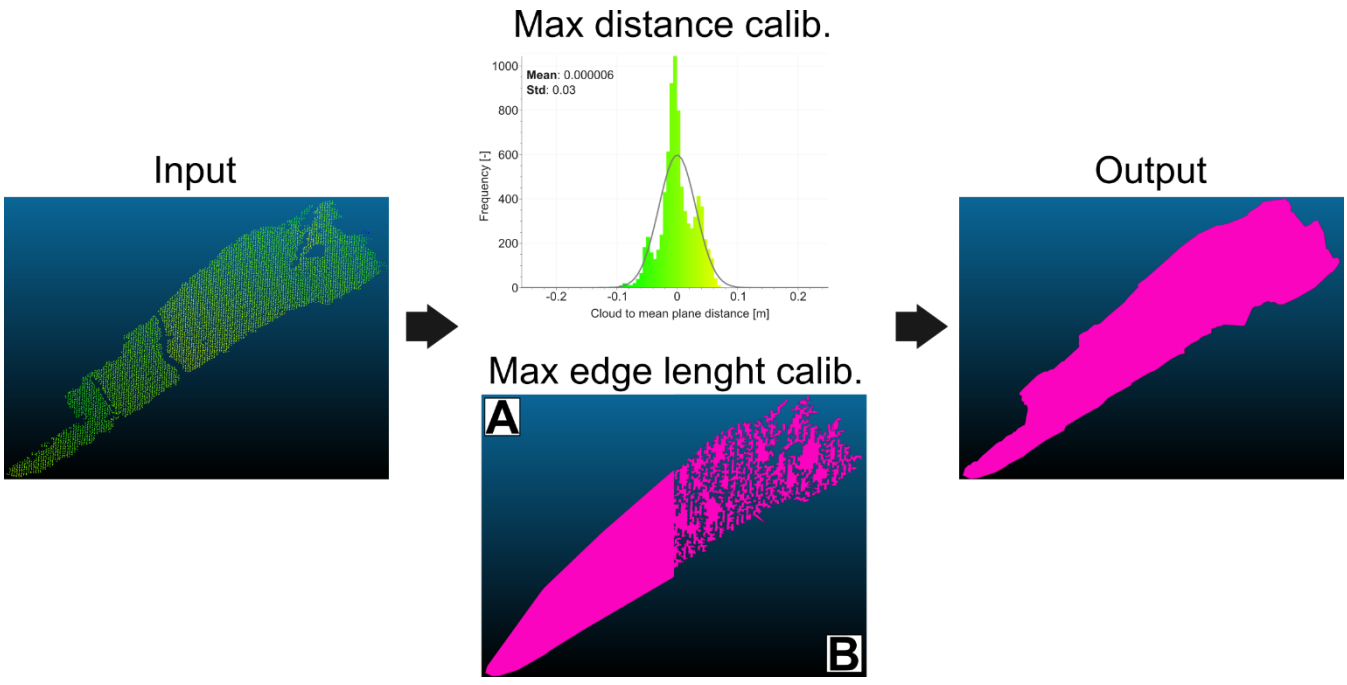

Figure 6 Example of the parameter calibration on a single facet. The max distance is calculated as the mean of the frequency distribution of the distances from the mean plane. (A) Example of a planar feature extraction when the max edge length parameter is too low. (B) When the max edge length is too high the planar feature results in a non-representative polygon. When the parameters are correctly calibrated the output planar feature precisely follows the point cloud border and no point is excluded from the interpolation for a too low max distance value.

4.5 Orientation parameters calculation

In structural studies of fracture networks, is common practice to assume that each fracture set shows an orientation distribution described by the unimodal circular symmetric Von Mises-Fisher distribution on a sphere (Fisher, 1953) - a specific declination of the more general Von Mises distribution (Mardia and Jupp, 2000) that, following a common practice in geological applications, will be called “Fisher distribution” in the following.

Even if it is sometimes reasonable to assume that fracture sets follow a distribution with circular symmetry, with the exception of particular situations like radial dikes and fractures formed in a flat layer before the onset of folding (e.g. Mandl, 2005), a statistical test is needed, particularly if the final goal is to use the results of orientation analysis in downstream simulations.

Fisher and Best (1984) proposed a goodness-of-fit test for the Fisher model, starting from a previous graphical test developed by the same authors (Lewis and Fisher, 1982). The poles of the family of n planes that need to be tested (I_j, D_j) with mean dip and direction $(\bar{I}, \bar{D})$, are rotated to obtain vectors with new coordinates (I_j', D_j'), with mean dip and dip

https://doi.org/10.5194/egusphere-2025-1398
Preprint. Discussion started: 11 April 2025

direction (0,0). The original vectors are than rotated a second time to obtain a new set of vectors (I_j'',D_j''). On these rotated values, the following derived datasets are tested:

- $S_E \equiv \{c_i' = 1 - \cos D_j', 1 \leq j \leq n\}$ (5)
- $S_U \equiv \{I_j', 1 \leq j \leq n\}$ (6)
- $S_N \equiv \left\{Z_i = D_j'' \sqrt{\sin D_j''}, 1 \leq j \leq n\right\}$ (7)

S_E is tested with the Kolmogorov-Smirnov test (Stephens, 1974) against an exponential distribution $E(1/k)$ to check the underlying colatitude distribution (exponentiality test). The Kuiper test (Stephens, 1974) is applied to test S_U against a uniform distribution $U(0,2\pi)$ to check the assumption of rotational symmetry around the mean vector (circularity test). The goodness-of-fit of S_N to a normal distribution $N(0,\sigma^2)$ is tested with the Kolmogorov-Smirnov test (Stephens, 1974) to check against the correlation between colatitude and longitude (normality test) (Figure 7).

Overall, this procedure provides a quantitative way to assess if the dataset can be fit with a Fisher model, allowing the calculation of the mean dip and dip direction of the cluster and the concentration parameter k.

https://doi.org/10.5194/egusphere-2025-1398
Preprint. Discussion started: 11 April 2025

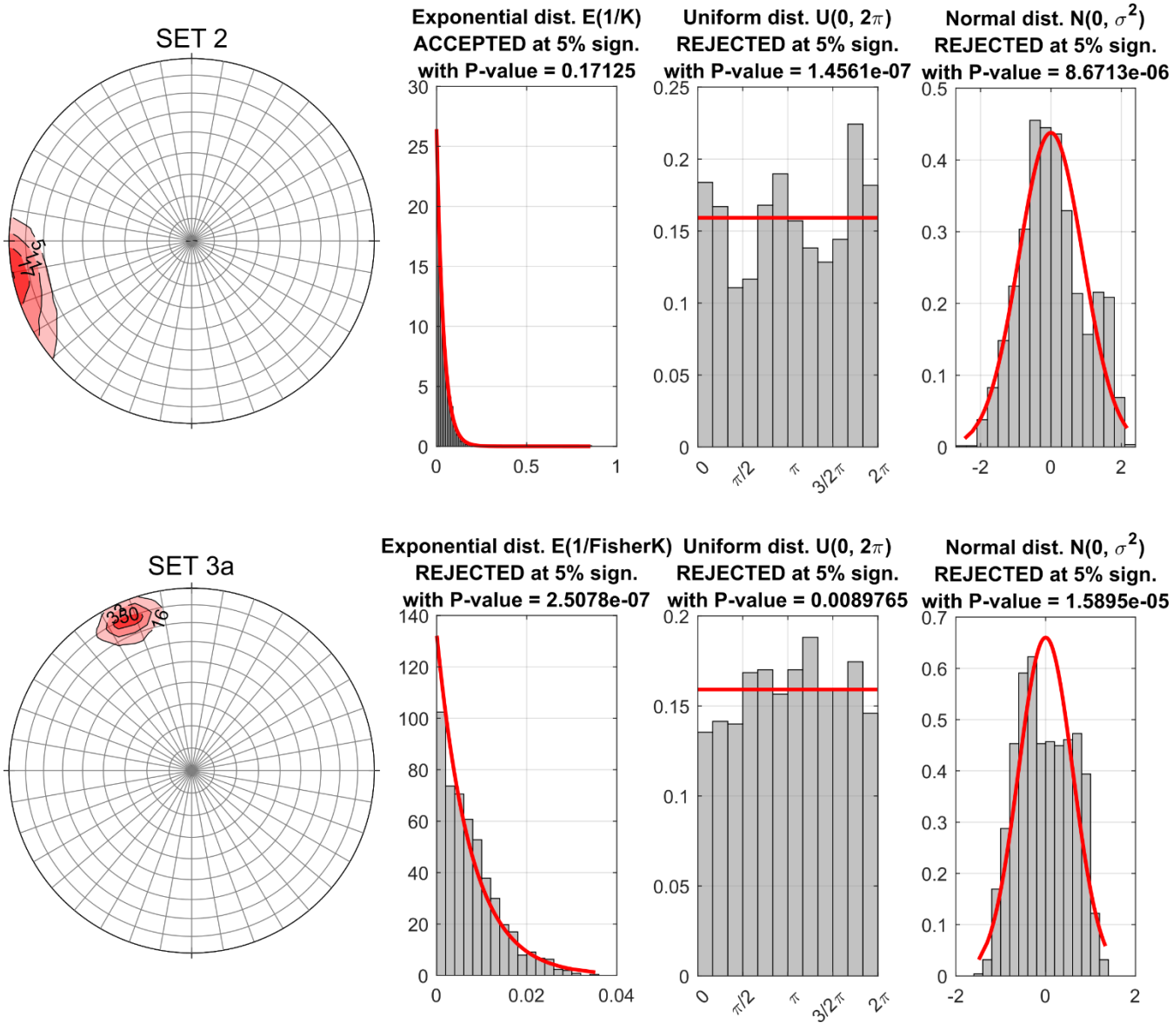

Figure 7 Example of the goodness-of-fit test for Set 2 and Set 3a of the Pontrelli quarry. The hypothesis of sphericity of the data is rejected based on all the tests.

If the Goodness-of-fit test is rejected, it is possible to fit a more general distribution. The Kent distribution is a natural extension of the Fisher distribution as it represents the analogue of a general bivariate normal distribution on a sphere (Kent, 1982). It includes the additional parameter β that describe the ovalness of the distribution, allowing to fit more elliptical clusters (Kent, 1982). No goodness-of-fit tests exist to check if the data follow the Kent distribution. Noteworthy, the Kent

https://doi.org/10.5194/egusphere-2025-1398
Preprint. Discussion started: 11 April 2025

model results in orientation distributions that are similar to those off the Bingham-5-parameter distribution (Kent, 1982), but has a different mathematical formula.

5 Enhanced interpretation on orthomosaic and DEM

Collecting orientation data directly from outcrops that lack a noticeable 3D morphological expression (i.e. the facets discussed above) is not possible. At the same time, measuring fracture size and intensity or density (length, height, P_{21}, etc.) from PC-DOMs is not reliable because facets do not correspond to complete fracture surfaces. For these reasons, we digitize fracture traces on TS-DOMs, obtained by projecting and merging the images collected during the photogrammetric survey onto a polygonal mesh or a DEM (in turn interpolated from the PC-DOM). This kind of data is different and complementary to what we discussed above, and only combining both kinds of information we can extract the most complete datasets from a DOM.

The dataset deriving from the interpretation of TS-DOMs is composed of an interpretation boundary (closed polygon) and a series of fracture traces (polylines) attributed to different fracture sets. The interpretation boundary limits the portion of the outcrop where fractures can be detected and digitized. It can include holes to isolate parts of the outcrop, covered by debris or vegetation, that are large enough to hinder the interpretation.

In this case study we were able to obtain orthophotos (see Section 3) of both the sub-horizontal pavement and of sub-vertical walls (Figure 2), and this allowed carrying out the fracture trace digitalization in a 2D GIS environment.

The availability of both RGB images and DEM (from which we can derive slope, aspect and hillshade), can allow following, with a better continuity, structures that may be challenging to detect in RGB only, due to alteration of the pavement surface, lack of colour contrast or zones damaged by quarrying activities, where longer fractures can still be digitized but are difficult to detect.

Every fracture set is saved in a dedicated file and every characteristic pertaining to a specific set is recorded into an attribute table field. For example, both set 1 and set 2 have both meso-faults and joints, this information is stored in an integer field coded as 1 for faults and 0 for joints. At the same time, set 3 is characterized by two main average orientations (Set 3a and Set 3b), but the fractures can be associated by their average length and abutting relationships with other sets. Fractures of Set 3a and 3b are than separated in a specific field.

Precise termination (snapping in GIS jargon) of abutting fracture traces is managed automatically, defining a threshold distance quantified in pixels. In the following sections we discuss how we characterize topological relationships, length/height distribution, H/L ratio and P_{21} from digitized fracture traces.

https://doi.org/10.5194/egusphere-2025-1398
Preprint. Discussion started: 11 April 2025

6 Fracture network topology

Due limitations imposed by observing them in outcrops, the topology of fracture networks, which are actually composed of fracture surfaces embedded in a 3D rock volume, is most of the times characterized in 2D, from fractures traces limited and/or connected by nodes (Dershowitz and Einstein, 1988; Barton et al., 1989; Renshaw, 1996; Manzocchi, 2002; Sanderson and Nixon, 2015; Sanderson et al., 2019). Even under this limitation, topology is a fundamental component of fracture network analysis because it is directly related to connectivity and fluid flow, as demonstrated by Sanderson and Nixon (2015).

Topological relationships are also instrumental in calculating unbiased length and height distributions, because topology allows identifying censored fractures by means of B nodes (Benedetti et al., 2025), and this also cascades into the estimation of the H/L ratio.

6.1 Standard topological analysis

From a topological point of view, a fracture network can be seen as a connected set of branches (fracture traces) and nodes (terminations and intersections), delimited by an interpretation boundary (e.g. defined by the natural limits of an outcrop). According to Benedetti et al. (2025), four main nodes categories can be found in a fracture network (Figure 8):

- I nodes: fracture trace true tip points;
- Y nodes: abutting relationship;
- X nodes: crosscutting relationship;
- V nodes: perfect coincidence of two tip points belonging to two different fractures - these are theoretically possible, but extremely unlikely;
- B nodes: boundary nodes, where a fracture trace terminates at the interpretation boundary.

The nature of I, Y, X and V nodes is related to the processes that generate the fractures in the first place, but an additional consideration pertains to B nodes (Nyberg et al., 2018, Benedetti et al., 2025), which result from the interaction between the fracture network and external processes. This interaction leads to the formation of false tip lines (false I nodes → B nodes) and the censoring of fracture traces. To prevent an underestimation of network connectivity, it is fundamental to exclude B nodes from the calculation of the relative proportions of I, Y, and X nodes.

Nodes classification is based on their topological value (Sanderson et al., 2019), representing the number of branches connected to each node. Specifically, I nodes have a topological value of 1, V nodes have a value of 2, Y nodes have a value of 3, and X nodes have a value of 4. B nodes can be categorized as nodes with a topological value of 3, but one branch originates from the fracture trace while the others come from the interpretation boundary.

FracAbility (Benedetti et al., 2025) is an easy-to-use original Python library developed for the quantitative statistical processing of fracture networks. Taking as input a set of polylines for each fracture set and a polygon representing the interpretation boundary, it is possible to obtain:

https://doi.org/10.5194/egusphere-2025-1398
Preprint. Discussion started: 11 April 2025

- IYX ternary diagram: the standard classification when it comes to topology (Figure 8A). In this diagram, the normalized distance from each vertex represents the relative frequency of I, Y and X nodes.
- Connectivity Index (CI): the mean number of connections per line, rendered as contour lines on the IYX ternary diagram (Manzocchi, 2002). As a reference, CI = 3.57 was defined as the critical CI for a constant length uniformly clustered system (Manzocchi, 2002).
- Backbone: the largest cluster of connected fractures in the network.

These results represent different aspects of the degree of connectivity of the fracture network. The ternary diagram and the connectivity index give information about the average connectivity of the network. Only when a fracture abuts on another one it is possible to reduce the number of I nodes in the network, thus moving towards the X and Y nodes vertices in the diagram means increasing, on average, the possibility to form large connected clusters within the network. However, the presence of clusters of connected fractures with a high connectivity index cannot be unravelled by the simple node count. Backbone extraction solves this problem, highlighting the more numerous connected cluster, and also represents a graphical solution to the percolation threshold problem, since if the backbone touches two opposite sides of the interpretation boundary, this means that a giant connected component exists, and a thoroughgoing flow can be established (Haridy et al., 2020). As shown in Figure 9, the backbone is marked by a significant increase in the CI value.

https://doi.org/10.5194/egusphere-2025-1398
Preprint. Discussion started: 11 April 2025

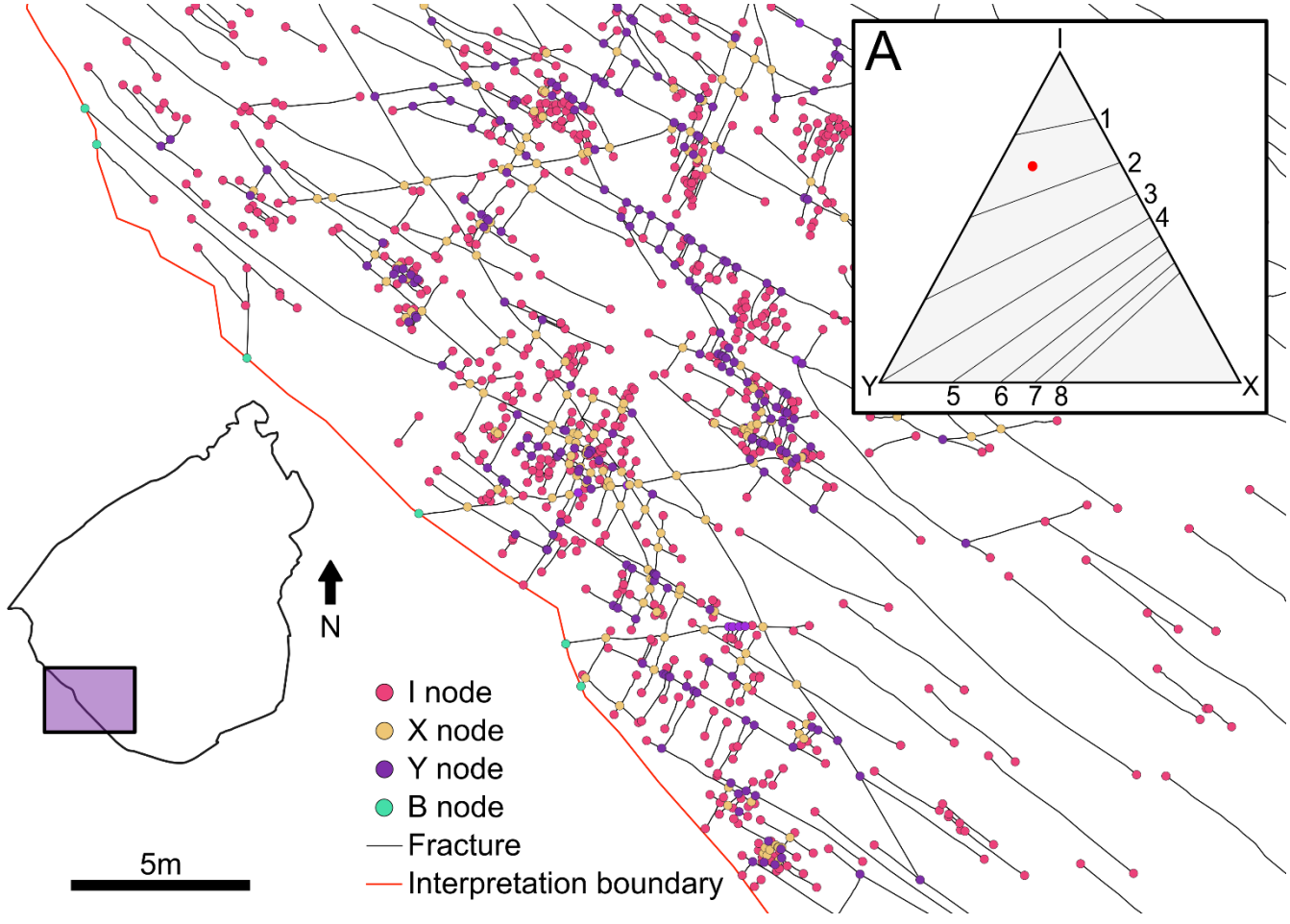

545

Figure 8 Topological relationship of the Pontrelli quarry fracture network. (A) Associated IYX ternary diagram, the red dot represents the connectivity index (CI).

https://doi.org/10.5194/egusphere-2025-1398
Preprint. Discussion started: 11 April 2025

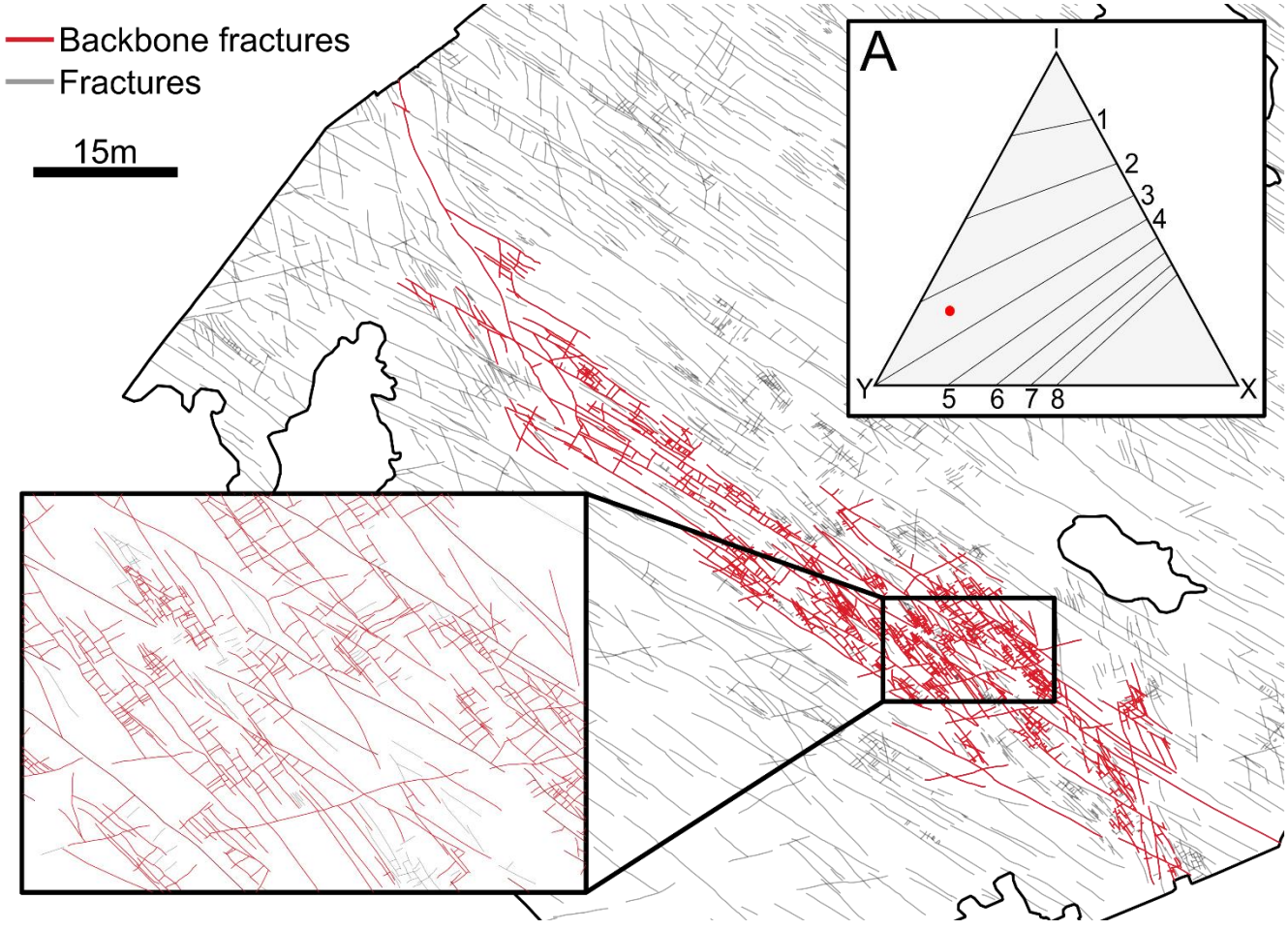

Figure 9 Backbone of the Pontrelli quarry fracture network. The backbone connects two sides of the pavement, indicating the presence of a giant connected component. (A) XYI ternary diagram of the backbone zone, the CI increase form 1.4 for the whole network to 3.5 along the backbone zone.

6.2 Directional Topology

Topological parameters presented in the previous section give a general picture of the fracture network as a whole and are calculated considering the fracture network as a single entity, not considering the geological classification of fractures in different sets (Figure 10A). It is thus impossible to retrieve information about a specific fracture set, for example, how many I, Y and X nodes a certain set have, or how a set is related to another one in terms of crosscutting and abutting relationships. This kind of information can be obtained with what we call "directional topology", where every node not only includes information about its type (I, Y, X and B), but also about its "origin" or "direction", i.e. from which sets a Y node is

https://doi.org/10.5194/egusphere-2025-1398
Preprint. Discussion started: 11 April 2025

generated and if it is the first fracture set that abuts on the second or vice versa. The same line of thought can be applied to X and I nodes but to a shallower level, given that in a crosscutting relationship it is not possible to define, just with topological information, which fracture is older or younger, and for I nodes it is only possible to identify the origin set.

To address this issue, when splitting fractures into branches to calculate topological values, FracAbility stores into the node attributes the set to which every branch belongs and the associated directionality (Figure 10B).

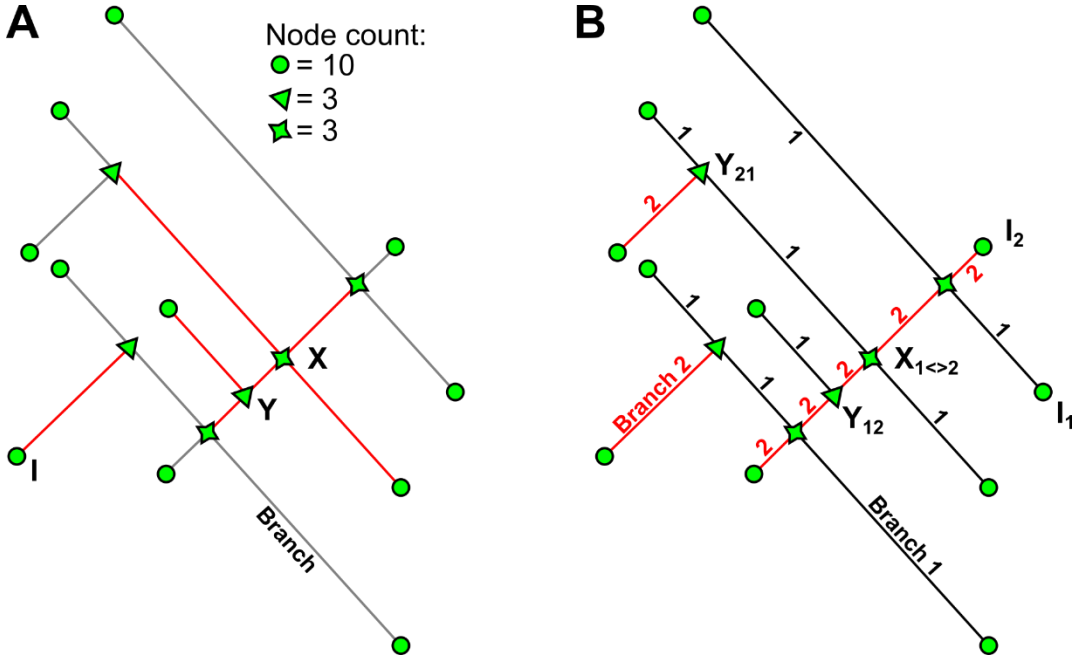

Figure 10 (A) Topological relationship based on the topological value for a fracture network composed of two fracture sets. Highlighted in red the necessary branches to define one specific node. (B) Topological relationship calculated taking into account the branch origin. X nodes are identified by the presence of two branches for every fracture set, Y nodes are identified by three connected branches. Of the three branches if only one pertain to a specific set it means that it is abutting on the other. I nodes are classified depending on the origin of the connected branch.

The usefulness of directional topology is not only limited to a more advanced description of the topological relationships within the fracture network, but can be also employed to define a quantitative parametrization of relative chronology between fracture sets, and of the stratabound versus non-stratabound nature of fractures.

In a hypothetical case where a fracture network is composed of two fracture sets, without censored terminations, and one of the two sets consistently abuts on the other, the abutting set will only show Y nodes. Thus, dividing the number of nodes by the number of fractures will yield exactly 2. In a real scenario, where the fracture network also includes censored fractures and B nodes, this result will be less than 2 because some of the Y-nodes are masked by censoring. To shield this relationship from censoring, it is necessary not only to subtract the number of censored fracture traces from the total, but also the number

https://doi.org/10.5194/egusphere-2025-1398
Preprint. Discussion started: 11 April 2025

of Y-nodes that represent the termination of a censored fracture trace from the total Y-nodes, defining the following relationship:

$$Fracture\ Binding\ Index = \frac{n_{Y\ nodes} - n_{Y\ censored}}{2\left(n_{frac.} - n_{frac.\ censored}\right)} * 100 = 100\% \quad (8)$$

where $n_{Y\ nodes}$ is the number of Y nodes of the abutting set, $n_{Y\ censored}$ is the number of Y nodes associated to a censored fracture (i.e. trace with one B node and one Y node), $n_{fractures}$ is the total number of fractures of the abutting set and $n_{frac.\ censored}$ is the number of censored fractures of the abutting set. The Fracture Binding Index (FBI) ranges from 0, when no fractures from the abutting set abuts on the other set, to 100% when every fracture is abutting on another fracture set. 100% of abutting nodes is an asymptotic value, very difficult to reach in a natural context, but nonetheless revealing a tendency in this direction would be interesting.

FBI can assume a different meaning depending on the context in which it is applied. In general FBI represents a quantitative way to assess relative chronology. In fact, considering two fracture sets, the one with the higher FBI is interpreted as being younger than the other one since it is consistently abutting. Moreover in vertical outcrops, if we consider the topological relationships between one fracture set and the bedding, FBI represents a quantitative parameter for the quantification of the tendency of a fracture set to be stratabound.

https://doi.org/10.5194/egusphere-2025-1398
Preprint. Discussion started: 11 April 2025

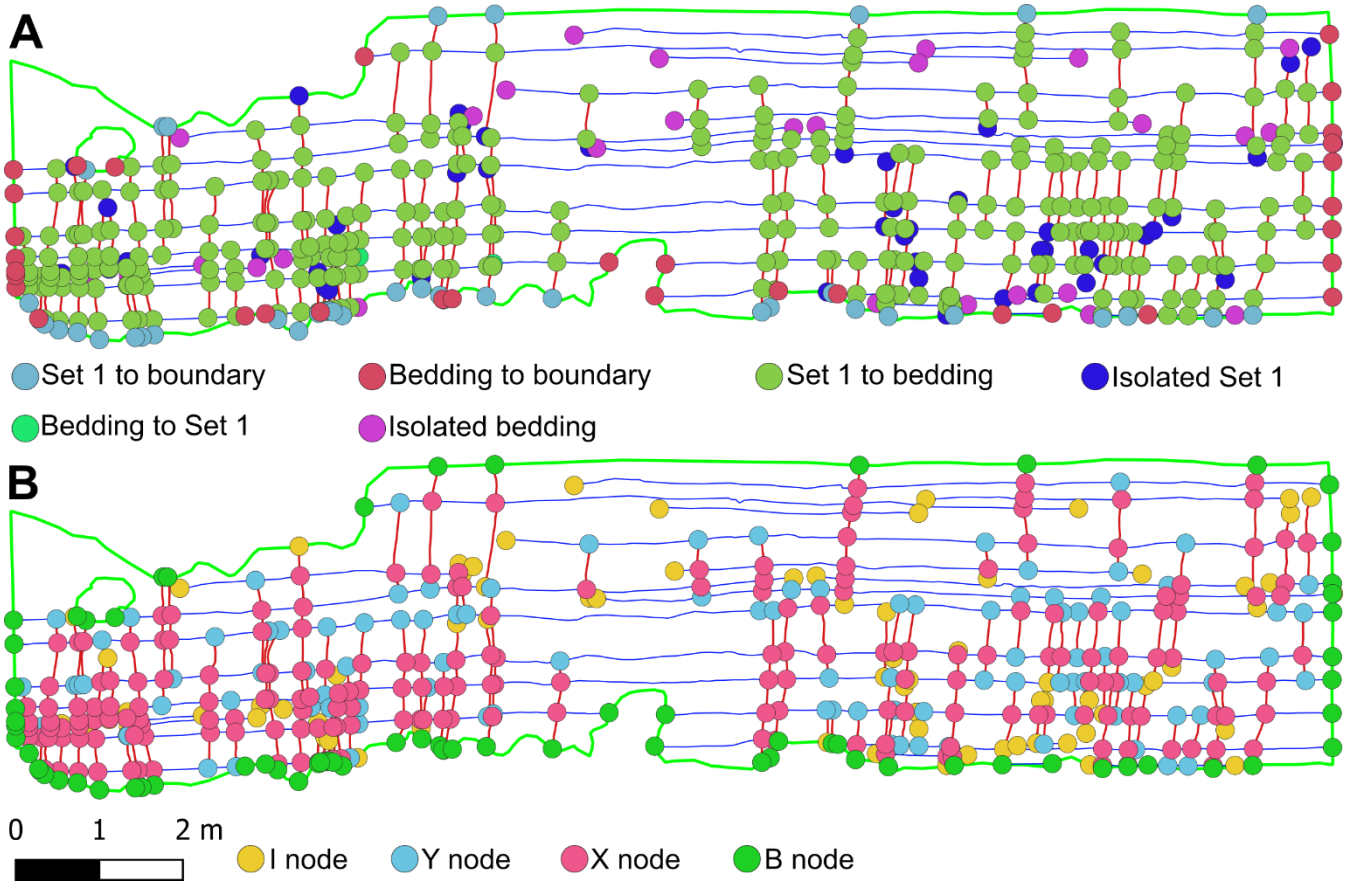

Figure 11 (A) Directional topology applied to Set 1 fractures on Pontrelli vertical wall (B) Standard topological classification of Pontrelli vertical wall. The complete topological characterization is given by the combination of A and B visualizations.

Figure 11 shows the application of directional topology to the Pontrelli vertical wall, considering Set 1 and the bedding (S). Applying the directional topology analysis we obtain:

- $n_{Y\ nodes} = 100$
- $n_{Y\ censored} = 28$
- $n_{frac.} = 93$
- $n_{frac.\ censored} = 40$

$$FBI_{1-B} = \frac{100-28}{2\,(93-40)_{.}} * 100 = 67\%$$

https://doi.org/10.5194/egusphere-2025-1398
Preprint. Discussion started: 11 April 2025

Therefore Set 1 is stratabound at 67%.

Considering now, for example, the abutting relationships of Set 3 on Set 1 as mapped in the pavement:

- $n_{Y\ nodes\ (3-1)} = 1161$
- $n_{Y\ censored\ (3)} = 4$
- $n_{\ frac.\ (3)} = 1863$
- $n_{frac.\ censored\ (3)} = 12$

$$FBI_{3-1} = \frac{1161-4}{2\ (1863-12)_.} * 100 = 31.2\%$$

On the contrary:

- $n_{Y\ nodes\ (1-3)} = 183$
- $n_{Y\ censored\ (3)} = 1$
- $n_{\ frac.\ (3)} = 2003$
- $n_{frac.\ censored\ (3)} = 175$

$$FBI_{1-3} = \frac{183-1}{2\ (2003-175)_.} * 100 = 4.9\%$$

Therefore Set 3 abuts with a FBI of 31.2% on Set 1, and on the other hand Set 1 abuts with only a marginal FBI of 4.9% on Set 3, which is considered just an effect of a few digitization errors or local deformational effects.

7 Trace length/height distribution

Defining an unbiased trace length distribution has always been one of the main challenges in rock mass and fracture network characterization. When calculating or estimating trace length parameters it is possible to distinguish between distribution-dependent and distribution-free methods (Mauldon, 1998). On one hand, distribution-free methods do not relay on any specific assumption about the underlying distribution, but provide an unbiased estimator of only the mean trace length by an indirect correlation (i.e. length is not physically measured, Warburton, 1980; Pahl, 1981; Kulatilake and Wu, 1984; Mauldon, 1998; Zhang and Einstein, 1998; Mauldon et al., 2001; Rohrbaugh Jr. et al., 2002). Not making assumptions about the shape and mathematical form of the distribution could be seen as an advantage, but actually the non-parametrical nature of these approaches implies that it is not possible to obtain important statistics of the population such as the standard

https://doi.org/10.5194/egusphere-2025-1398
Preprint. Discussion started: 11 April 2025

deviation without imposing further assumptions (Pahl 1981). This makes distribution-free methods unsuitable for modern modelling applications, such as stochastic generation of fracture network, where a fully specified distribution is required. On the other hand, distribution-dependent methods make assumptions on the shape of the underlying trace length distribution, thus constraining their results. Because of this, it is necessary to test how well the chosen distribution fits the data. In the past this was a strong limitation, due to the biases discussed in Section 1.

Digital outcrops make it possible to overcome with huge datasets some problems that previous authors could only consider theoretically from a mathematical and stereological point of view. With these new techniques it is possible to acquire massive datasets on very large sampling windows and successfully tackle the different biases that can be present on an outcrop.

The orientation bias can be treated by applying areal sampling on outcrops with perpendicular faces. All the fracture sets perpendicular or sub-perpendicular to the horizontal plane are detected on the pavement. If present, fracture sets parallel to the horizontal pavement can be measured on the perpendicular vertical wall, eliminating the issue of under-sampling fracture sets with unfavourable orientations.

The size bias applies to 1D sampling methodologies (scanlines) where longer fractures have a higher probability of being sampled, but this bias does not apply to areal sampling strategies where everything inside the interpretation boundary is sampled. Even fractures much longer than the interpretation boundary are sampled and classified as censored fractures (see below).

Working with DOMs, the truncation bias applies to small fractures that can be truncated by limited DOM resolution. In our case, the resolution of the TS-DOM is around 4 mm/pixel and the smallest digitized fracture is 57 cm. This means that there is an order of magnitude between the two and it can be safely assumed that truncation bias is not affecting the dataset.

Consequently, the only remaining bias to be treated is the censoring bias, which occurs naturally due to the finite nature of the outcrop or the presence of vegetation or debris. In statistics, censoring is a condition where the value of a measurement is partially known. This occurs when some of the data are subject to limitations or restrictions, preventing us from observing the complete information. Censoring can happen for various reasons, and it is a common scenario in statistical analysis (Kaplan and Meier, 1958; Leung et al., 1997; Lawless, 2011). In our case, the fractures that touch the interpretation boundary are objects whose length is partially measured, therefore affected by random censoring (Benedetti et al., 2024).

We thus apply the theory and approaches described in Benedetti et al., (2024) to obtain an unbiased statistical model from censoring of both the length and height distributions. As discussed in Benedetti et al., (2024), this analysis solves the problems related to single censoring, double censoring, and those related to “holes” within the interpretation boundary, as depicted in Figure 12.

https://doi.org/10.5194/egusphere-2025-1398
Preprint. Discussion started: 11 April 2025

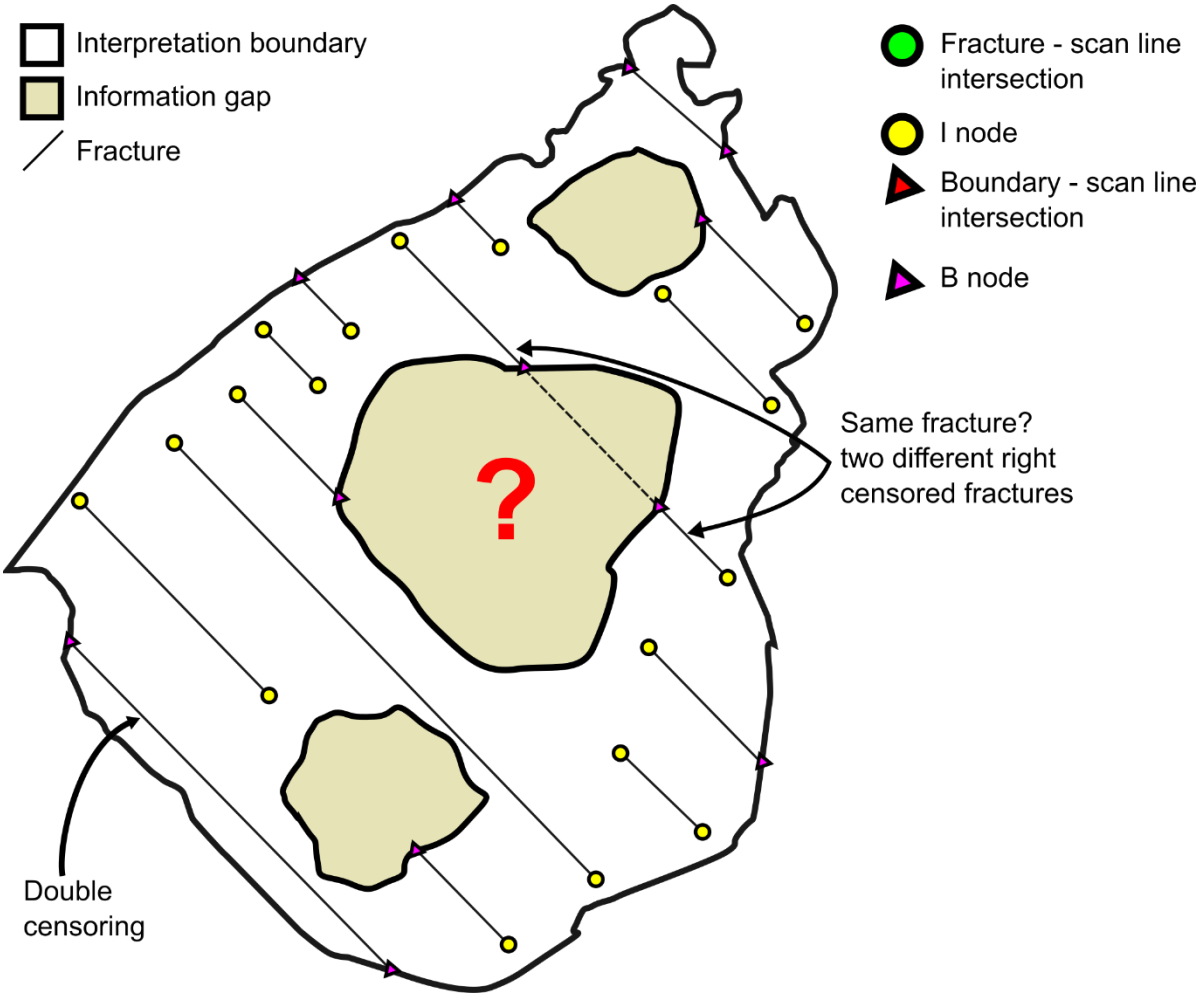

Figure 12 Different cases of censoring in a natural outcrop. The presence of information gaps affects trace length measurements. Double censored fractures are considered a single censored fractures with one of the end nodes coinciding with the interpretation boundary.

Survival analysis parameter estimation is based on optimization algorithms, like the Maximum Likelihood Estimation (MLE), where censoring is taken into account by calculating the likelihood of a censored measurement by using the survival function instead of the probability density function (Benedetti et al., 2024). MLE is a parametric approach that needs a testing phase to validate its results. Working with censored data, without a specified distribution, leads to a situation where none of the standard non-parametric goodness-of-fit test can be applied (Benedetti et al., 2024).

Using the survival analysis approach different hypothesis (statistical models) can be estimated with the censored data. For this case study we propose to fit the following statistical models: Lognormal, General Gamma, Weibull, Exponential, Gamma, Logistic and Normal. Several statistical distances are calculated between the available empirical data and the fitted model to show which of the proposed models is more representative of the data. We chose to use the same distances as (Benedetti et al, 2025) thus using: Kolmogorov-Smirnov distance (DC_n) (maximum distance), the Koziol-Green distance

https://doi.org/10.5194/egusphere-2025-1398
Preprint. Discussion started: 11 April 2025

(Ψ_n^2) (sum of squared distances) and the Anderson-Darling distance (AC_n^2) (weighted sum of squared distances), with respect to a uniform distribution U(0,1) (2) Akaike information criterion (Benedetti et al., 2024).

7.1 Distance from U(0,1)

The probability integral transformation theorem (Fisher, 1930) is a fundamental concept in probability and statistics, whose primary application is to transform the values of a random variable into a random uniform variable. The perfect model for fitting a dataset will follow a uniform distribution between 0 and 1, meaning a perfect correspondence between the empirical data and the theoretical distribution, and other models that are close to the uniform U(0,1) with a small deviation will be suitable to describe the data (Figure 13). Therefore, the purpose of the probability integral transformation is to normalize distributions in order to be able to compare deviations on a common ground.

Table 3 show the rankings based on the different normalized distances for Set 1 fractures. The lognormal distribution and the general gamma distribution rank respectively first and second in all the 3 rankings. In contrast, the logistic and the normal distribution are not suitable for our data. With intermediate rankings, we can appreciate the different meaning of the various distances; for example, the Weibull distribution shows a smaller maximum distance (DC_n) with respect to the exponential and the gamma distribution.

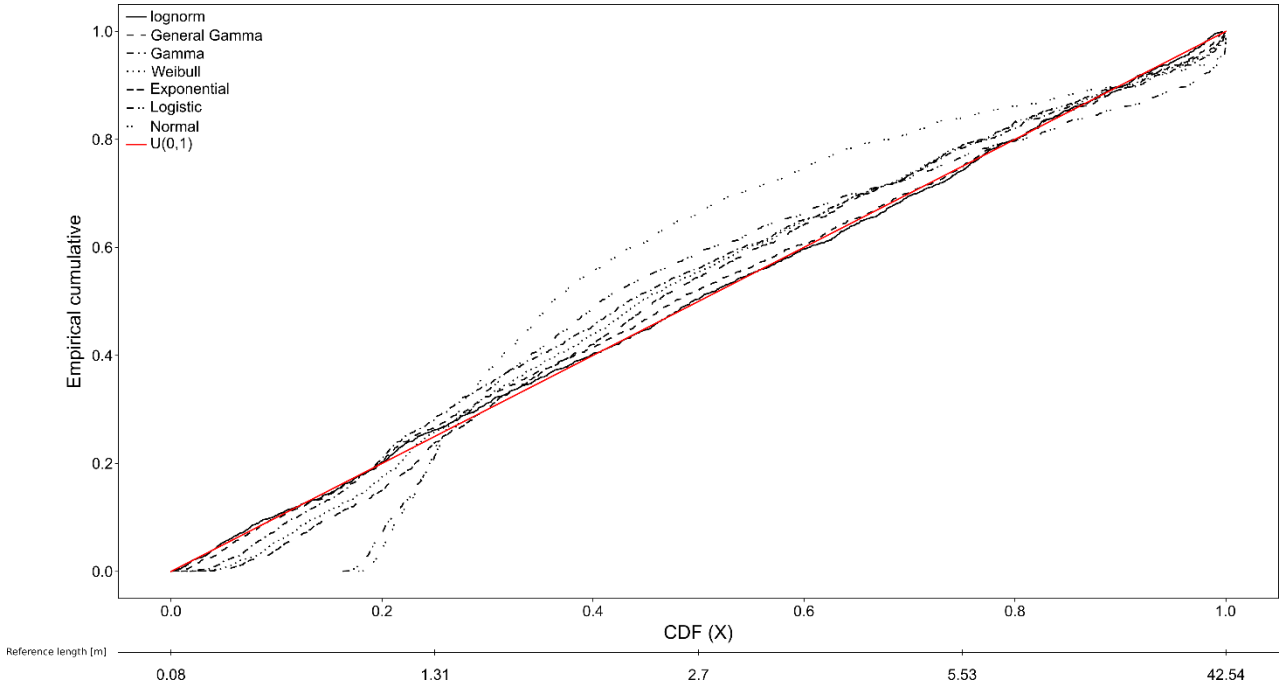

Figure 13 PIT visualization for Set 1 fractures.

Name	DC_n rank	Ψ_n^2 rank	AC_n^2 rank	Mean rank
Lognormal	1	1	1	1

https://doi.org/10.5194/egusphere-2025-1398
Preprint. Discussion started: 11 April 2025

General Gamma	2	2	2	2
Weibull	3	4	3	3.33
Exponential	4	3	5	4
Gamma	5	5	4	4.67
Logistic	6	6	6	6
Normal	7	7	7	7

Table 3 Ranking based on the Kolmogorov-Smirnoff distance, Koziol-Green distance and Anderson-Darling distance for Set 1 trace length data.

7.2 Akaike information criterion

The Akaike information criterion (AIC), is a criterion to rank models from the best to worst based on the empirical data (Akaike, 1974; Burnham and Anderson, 2004). AIC is designed to identifying the so called MAICE (Minimum information theoretic criterion (AIC) Estimate) (Akaike, 1974), as the model that give the minimum of AIC, defined as:

$$AIC = 2k - 2ln(L_{max}) \quad (9)$$

Where:

- k: number of model parameters
- L_{max}: maximized value of the likelihood function

Therefore the Akaike Information Criterion favours parsimony, preferring models with fewer parameters that still adequately explain the data (Akaike, 1974).

Associated to AIC, there is another important parameter that gives the probability that a certain model is the best model for a given dataset, the Akaike weights (w_i) (Burnham and Anderson, 2004). These sum to 1 and have to be interpreted as a weight of evidence, meaning that the higher the value, the higher the probability that a certain model, in the pool of the selected models, is the best model for our data (Benedetti et al., 2024).

The main advantage of this method is that it takes as input the maximized value of the likelihood function, de facto ranking models and their relative parameters taking into account censored data.

Rank	Distribution name	AIC	w_i
1	Lognormal	7514.617939	0.9912701876
2	General Gamma	7524.082426	0.0087298124
3	Gamma	7636.568978	0
4	Weibull	7653.734152	0
5	Exponential	7655.821815	0

https://doi.org/10.5194/egusphere-2025-1398
Preprint. Discussion started: 11 April 2025

6	Logistic	8804.536054	0
7	Normal	9246.922169	0

Table 4 Ranking based on the Akaike information criterion for Set 1 trace length data.

Just looking at AIC values (Tab.4), and at the various distances measured in the previous section, it seems that even if the lognormal distribution wins, the three-parameters general gamma distribution is still a valid model for our data. Akaike weights clarify this situation showing that the lognormal model is much more powerful at describing our data with respect to the gamma model. At the same time, all the other models have Akaike weight equal to 0 meaning that with respect to the lognormal and the General gamma models, they are completely unsuitable.

8 Fracture areal intensity (P_{21})

Fracture areal intensity is defined as the ratio between the total sum of fracture trace length and the sampling area (Dershowitz and Herda, 1992; Mauldon et al., 2001). This parameter is very important since its volumetric equivalent P_{32} (total fracture area in unit volume) is used as a stopping criterion in stochastic DFN modelling, meaning that the stochastic generation of fractures will stop when the target intensity is reached, and P_{32} can be obtained form P_{21} via a calibration procedure (Staub et al., 2002). Given the heterogeneous distribution of fractures in natural outcrops, the characterization of this value cannot be separated from the concept of Representative Elementary Volume (REV) or Area (REA) (Bear, 1975). In outcrop studies REA is the area above which a certain parameter value becomes independent from the position and scan area size with which it is calculated and thus the value can be used to constrain wider models.

To perform this analysis limiting the orientation bias we cover the outcrop surface with hexagonal grids of increasing edge length, ranging from 1m to 26m in the Pontrelli quarry case study. Only whole hexagons are considered and data are plotted using the graphical boxplot method proposed by Tukey, 1977 (Figure 14A). The lower threshold of REA can be defined as the minimum hexagon area where no significant difference is detected between the mean and standard deviation of P_{21} obtained at that area and at the next step.

To quantitatively measure the significance of this difference, statistical techniques like ANOVA, used to compare the mean of different populations, can be used in theory (Stahle and Wold, 1989; Moder, 2010). However, ANOVA is based on three assumptions: (i) hypothesis of normality, (ii) homogeneity of variances, (iii) independence between samples (Moder, 2010). In our case, P_{21} samples collected with smaller scan areas are clearly asymmetrical (from 1m to 5m), while P_{21} samples collected with larger scan areas tend to be more symmetrical (Figure 14A). Consequently, variance is inhomogeneous through the dataset, leading to an increase of type 1 errors (Moder, 2010). This problem is enhanced by the fact that the sample size is unequal and decays as the scan area edge length increases due to the finite size of the outcrop (the larger the outcrop, the smaller the number of scan areas). For these reasons, ANOVA and similar tests cannot be applied, and we decided to adopt a more qualitative approach based on the difference between the interquartile range (deltaIQR) of two subsequential P_{21} samples. With this approach, REA is reached when deltaIQR stabilizes around 0 (Figure 14B). To account

https://doi.org/10.5194/egusphere-2025-1398
Preprint. Discussion started: 11 April 2025

for "far out" data, that are not included in the IQR, we also consider the range between the whiskers calculated as the difference between the upper whisker length (Q3 +1.5IQR) and the lower whisker length (Q1 - 1.5IQR) (Figure 14C).

In both cases, REA correspond to a plateau that in our case study between 5m and 12m of scan-area edge length. Above 12m, the representativity is compromised by the too small sample size (<15 hexagons).

P_{21} REA can be safely calculated only for Set 1 fractures, because, as highlighted in Section 2, in some areas only Set 1 fractures can be digitized, while Set 2 and Set 3 are drowned by the quarrying related fractures.

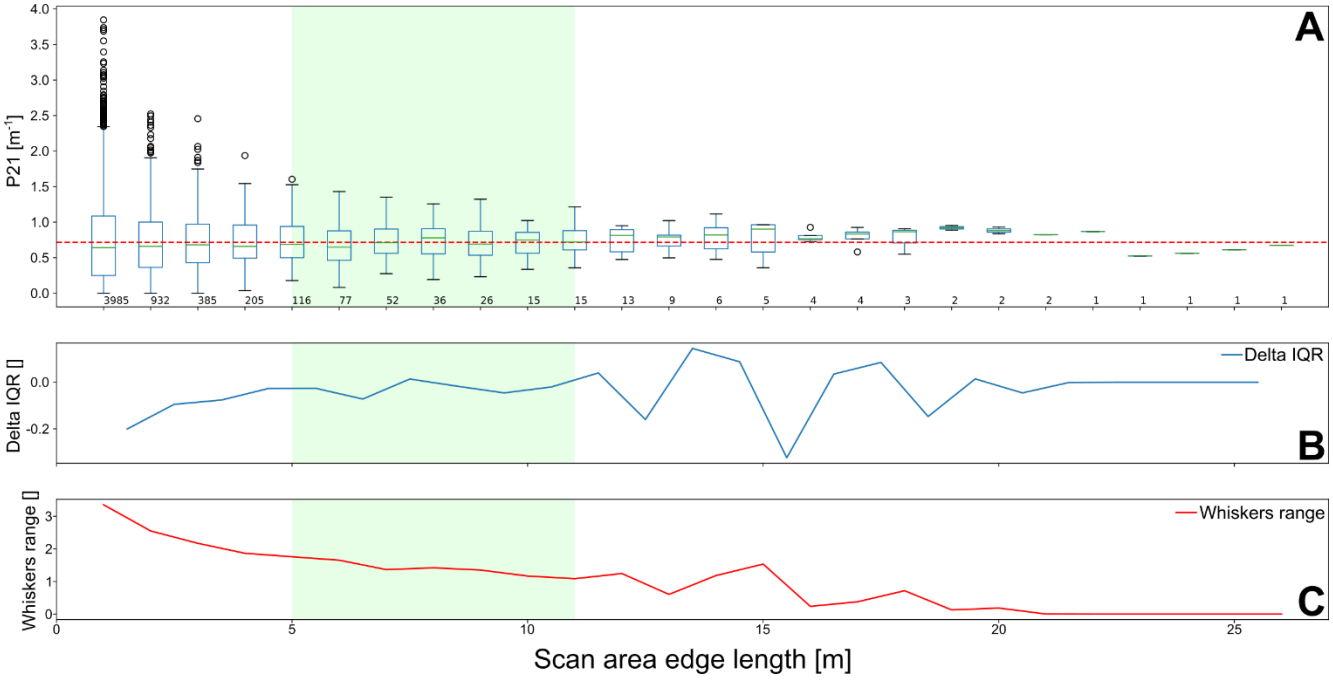

Figure 14 Representative Elementary Area analysis on Pontrelli quarry Set 1. (A) Boxplot of P_{21} data collected with increasing scan area size. Red dashed line: P_{21} calculated on the whole outcrop, with the interpretation boundary as scan area. Green box identifies REA range. Small number under the boxplot: sample numerosity. (B) Delta between IQR of two subsequential P_{21} samples. (C) Range between upper and lower whiskers for each P_{21} sample.

9 Height/Length ratio

The H/L ratio between height of fractures, measured along the dip direction, and their length, measured along strike, is the object of an extensive literature and is believed to span from 1:2 (Odling, 1997; Panza et al., 2015; Giuffrida et al., 2020), to 1:4 (Panza et al., 2015) or even 1:5 (Boro et al., 2014; Smeraglia et al., 2021), depending and different mechanical hypotheses, but could be probably even more variable when crosscutting/abutting relationships between fracture sets and with bedding are considered.

H/L ratio is applied, in association with the length distribution, in most commercial and open-source 3D stochastic DFNs to model the geometry of the discontinuities, often represented as rectangular or elliptical surfaces. Therefore, the H/L ratio is directly correlated to the shape of the fracture planes generated by the DFN and it is responsible for the jump in

https://doi.org/10.5194/egusphere-2025-1398
Preprint. Discussion started: 11 April 2025

dimensionality between 2D and 3D models. Unfortunately, the H/L ratio cannot be directly measured in outcrops due to the impossibility to map the full extension of fracture surfaces (but only their traces or partial facets).

In the studied outcrop, the availability of both height and length data allows us to make at least some realistic and transparent assumption on the H/L ratio based on a correlation of length and height distributions.

Our assumption is that traces mapped on the pavement (i.e. lengths) and on the wall (i.e. heights) can be associated in ordered pairs from the shortest to the longest. Making some assumption of this kind is unavoidable since there is no way to directly observe the correspondence between horizontal and vertical traces. We want to stress that this criterion is not unique, and other relationships can be established between length and height data (e.g., random association), but this criterion seems reasonable from a fracture mechanics point of view.

To test our hypothesis, a hundred values of length and height are randomly sampled from the statistical distributions of length and height, ordered from smallest to largest and associated in pairs, and the H/L ratio is eventually obtained with linear regression (Figure 16A).

In our case study the height of Set 1 fractures should be limited by the height of the bed package, but the random sampling of the height distribution, that is a lognormal distribution, also generates, although with decreasing probability, fractures that are much higher. This is why in Figure 15 we limited the linear regression to height values smaller than 6m (height of bed package, Panza et al., 2016). One thousand realizations are made to account for the variability of the random sampling and the arithmetic mean of the regression line is taken as the representative H/L ratio (Figure 15B).

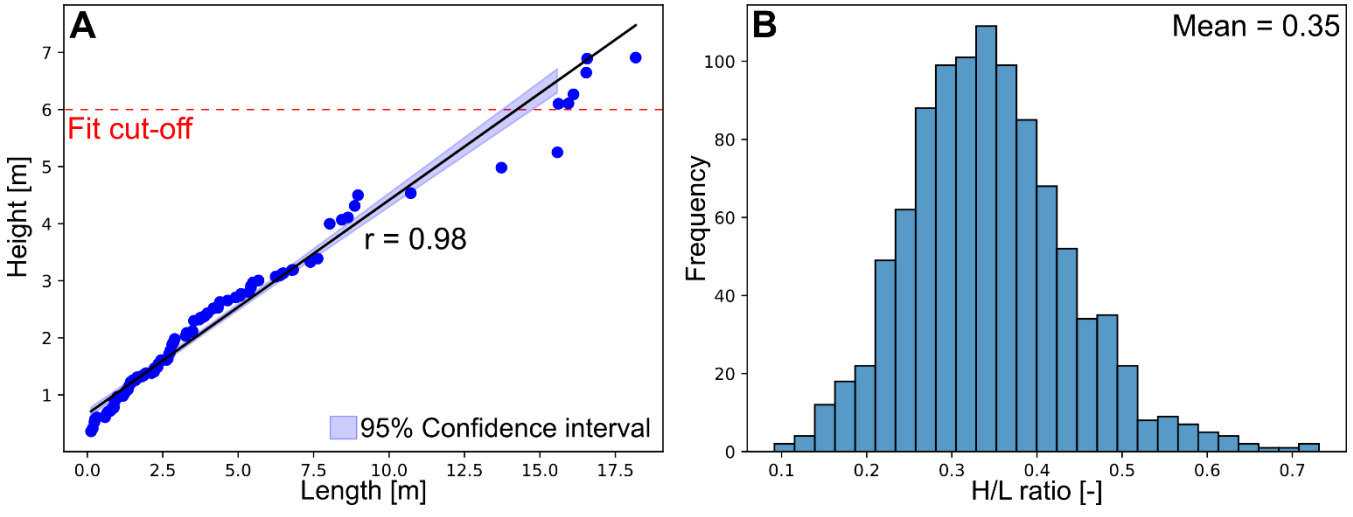

Figure 15 H/L ratio calculated for Set 1 fractures. (A) Example of one realization, where hundred values are sampled from the height and length distributions. r: Pearson correlation coefficient. (B) Frequency histogram of H/L ratios calculated from thousand realizations.

https://doi.org/10.5194/egusphere-2025-1398
Preprint. Discussion started: 11 April 2025

10 Summary of the results: fracture network characteristics at the Pontrelli quarry

In this section we describe the fracture network of the Pontrelli quarry and the results and limitations of the parametrization obtained with our workflow. Field observations show that Set 1 is the most prominent set in the outcrop, its fracture traces are homogeneously distributed across the pavement, and it can be detected even in areas damaged by quarrying. From field and DOM evidence, all other fracture sets abut or crosscut Set 1, therefore pinpointing this set as the older one. This conclusion is also supported by the topological, length and height analyses. Set 1 shows a lognormal length distribution with the largest average and maximum length, in agreement with a condition in which fractures are free to grow, in absence of a mechanical compartmentalization defined by previously developed fracture sets, bedding aside (Ackermann and Schlische, 1997). Set 1 also shows a negligible percentage of abutting relationships with Set 2 (2.7%) and Set 3 (4.9%). This marginal number of unlikely relationships, in a geological context in which Set 2 and Set 3 postdate Set 1, can be explained considering a limited reactivation of Set 1 fractures in more recent tectonic phases. On the contrary, both Set 2 and Set 3 exhibit a significant number of abutting relationships against Set 1, respectively 21.41% and 31.2%.

The favourable orientation of the vertical wall supports the collection of a consistent statistical sample of height measurements, allowing for a robust fit of the height distribution. However, the height of the vertical wall is barely sufficient to get a complete observation window on a bed package. This limits the representativity of the assumption on the stratabound nature of Set 1. Our interpretation relies on the results from the directional topology analysis between Set 1 and the bedding. Since more than 67% of the observed Set 1 fractures abut on bedding surfaces, we believe that it should be vertically confined by the height of the bed package. H/L ratio for set 1 is calculated as discussed above from the trace height and length distributions, under the assumption that height and length values are associated in pairs from smallest to largest. This assumption is supported by the strong linear correlation between the two sets of values (Figure 15) and the resulting H/L ratio is 0.345.

Set 1							
	Test result	**Mean dip dir.**	**Mean dip**	**Fisher K**	**Kent K**	**Kent β**	**n. data**
Orientation	rejected	213.94	86.3	36.59	39.59	5.42	1475

	Set 2	**Set 3**	**S (Bedding)**
FBI	2.70%	4.9%	67%

	Dist. Type	**Mean**	**Standard dev.**	**n. data**
Length distribution	Lognormal	4.49	6.03	2014
Height distribution	Lognormal	2.09	1.69	93

https://doi.org/10.5194/egusphere-2025-1398
Preprint. Discussion started: 11 April 2025

H/L ratio	0.345	

	Value	**REA**
P_{21}	0.7 m-1	5-12m

Table 5 Result summary for Set 1 fractures.

Set 2 mean length is intermediate between Set 1 and Set 3 and the topological relationships exhibit a higher occurrence of Y nodes against Set 1 with respect to Set 3, in good agreement with Set 2 being the second older set. The orientation of the vertical wall still allows to collect both faces and traces of Set 2 fractures, albeit the trace height dataset is less numerous than for Set 1, resulting in a less constrained height distribution. This is also reflected in the H/L ratio calculation, which should be applied more cautiously to stochastic modelling.

Unlike Set 1, Set 2 fracture traces in the northern part of the outcrop are drowned by the damaged zones and the noise generated by quarrying activities. There is a reasonable doubt that Set 2 fractures are really not present in that part of the quarry, but faces and traces data collected on the wall prove otherwise. The incomplete sampling of fracture traces across the pavement defines a strong bias that hinders the calculation of the P_{21} for Set 2, since without a sufficiently wide sampling area the REA calculation is not representative. Therefore, if we would model this fracture set with a stochastic approach, some assumption on the REA must be introduced.

Most of Set 1 and 2 fractures on the vertical wall abut on bedding surfaces. This imply that bedding surfaces, in this context, actually have a control on the vertical development of the fractures. This is particularly true for the "high order" bedding surfaces that limit the bed package, where almost 50% of Set 1 fractures abut.

Set 2							
	Test result	**Mean dip dir.**	**Mean dip**	**Fisher K**	**Kent K**	**Kent β**	**n. data**
Orientation	rejected	75.37	89.31	26.47	27.91	3.1	1933

	Set 1	**Set 3**	**S (Bedding)**
FBI	21.41%	9.69%	97.91%

	Dist. Type	**Mean**	**Standard dev.**	**n. data**
Length distribution	Lognormal	2.094	2.2	913
Height distribution	Lognormal	1.3	0.78	32

H/L ratio	0.359

Value	REA

https://doi.org/10.5194/egusphere-2025-1398
Preprint. Discussion started: 11 April 2025

P_{21}	\	\

Table 6 Result summary for Set 2 fractures.

Set 3 shows the highest number of abutting relationships against the other sets and the smallest average length, in agreement with Set 3 being the younger represented on this outcrop.

Given the unfavourable orientation of the vertical wall (sub-parallel to Set 3 average attitude), only orientation data from facets can be collected and the height distribution cannot be characterized. This implies that also the H/L ratio cannot be obtained. Finally, regarding P_{21} and REA, the same limitations as for Set 2 apply. Therefore, in case we would model this fracture set with a stochastic approach, many relevant assumptions must be introduced even if in general the quality of the outcrop is very high.

Set 3							
	Test result	**Mean dip dir.**	**Mean dip**	**Fisher K**	**Kent K**	**Kent β**	**n. data**
Orientation (Set 3a)	rejected	157.46	78.75	132.83	133.52	4.45	1269
Orientation (Set 3b)	rejected	124.08	76.8	91.83	92.63	4.2	2123

	Set 1	**Set 3**	**S (Bedding)**
FBI	31.2%	21.19%	\

	Dist. Type	**Mean**	**Standard dev.**	**n. data**
Length distribution	Lognormal	0.74	0.75	1863
Height distribution	\	\	\	\

H/L ratio	\

	Value	**REA**
P_{21}	\	\

Table 7 Result summary for Set 3 fractures.

11 Discussion

This contribution proposes a workflow with quantitative methodologies to address the parametrization of fracture networks aimed, for instance, to the generation of stochastic models that are more realistic under the geological and structural point of view. Our approach is based on a combination of traditional field surveys and DOM surveys, the latter used to obtain large datasets to support statistical analysis, the former to guide the digital mapping, filtering the noise given by external factors

https://doi.org/10.5194/egusphere-2025-1398
Preprint. Discussion started: 11 April 2025

(e.g. quarrying operations) and assigning every fracture to a specific set through geological observations (particularly kinematics and relative chronology).

Filtering noise and associating a genetic signature to each fracture set is an obvious concern in a quarry, where some fractures were generated during quarrying operations, but is of the outmost importance also in an outcrop analogue modelling perspective, if for instance we want to filter out fractures generated during exhumation, that might not be present in a reservoir still buried at depth.

The very high quality of our outcrop, with perfectly exposed horizontal and vertical surfaces, was instrumental in testing techniques that represent, in our opinion, a step forward in collecting rich quantitative datasets and developing rigorous statistical treatments for many parameters of a fracture network (Table 1). On the other hand, we must also recall that for some parameters there are still limitations in data collection and analysis. Both these points are discussed in the following sub-sections.

11.1 Combined analysis of fracture traces and faces

The integration of facets and traces (collected both on horizontal and vertical outcrops) allows a complete characterization of fracture network parameters, unlike other approaches that rely on the analysis of only one of these two datasets (e.g. Ortega et al., 2006; Boro et al., 2014; Martinelli et al., 2020; Smeraglia et al., 2021).

Orientation data have been collected on the vertical wall PC-DOM, where dip and dip direction of true 3D planes can be measured by fitting a mean plane to planar patches of the point cloud.

TS-DOMs allow the digitalization of fracture traces and of the interpretation boundary both on horizontal and vertical outcrops. The integration between fracture traces and the interpretation boundary is fundamental to avoid underestimating the connectivity index by misinterpreting B-nodes as I-nodes, and provides a fundamental input to identify censored fractures.

P_{21} is calculated on the pavement TS-DOM where the huge areal extension enables to define a sufficient number of scan areas to detect the REA lower threshold.

11.2 Orientation analysis

The methodologies we suggest for orientation analysis are aimed at reducing subjective choices of the interpreter and at the same time exploiting semi-automatic data collection to increase the volume of data that support statistical analysis. This was achieved by:

- Introducing cluster analysis, in addition to classical structural observation, to segment fracture sets following a robust statistical criterion.
- Calibrating an automatic feature extraction algorithm (FACETS) to maximize the data that can be extracted from PC-DOMs, avoiding the generations of artifacts (e.g. planes with an intermediate orientation) as sometimes happens in workflows tested by previous authors (e.g. Menegoni et al., 2019; Panara et al., 2024).

https://doi.org/10.5194/egusphere-2025-1398
Preprint. Discussion started: 11 April 2025

- Testing the fitted orientation distributions with goodness-of-fit tests, instead of assuming circular symmetry and a Fisher distribution without a proper statistical test as (unfortunately) is a common practice in structural geology (e.g. Bisdom et al., 2014; Smeraglia et al., 2021; Menegoni et al., 2024; Panara et al., 2024, just to cite some recent papers).

Our rigorous analysis revealed that, in our case study, no fracture set follows a Fisher distribution (Tab.5, 6, 7), in contrast to the conclusions of previous studies on the same outcrop (Panza et al., 2016; Zambrano et al., 2016). At the same time, Kent distribution parameters indicate a very low ovalness for all fracture sets, even if Set 3a and Set 3b seem to be almost elliptical clusters (Fig 5e). The reason is that sets 2, 3a, and 3b are strongly asymmetrical and set 1 is multimodal, as highlighted by contour plots in figure 5.

In the context of generating analogue fracture sets with stochastic modelling (e.g. in DFN), where only the Fisher distribution can be modelled by standard software, these parameters should be handled with care. Using a Fisher distribution with a K parameter small enough to fit all the planes in the cluster (i.e. with a large spherical variance) will result in artifacts along the minimum axis of the elliptical distribution, or in not properly represented tails in case of asymmetrical distributions. On the contrary, using a K parameter that is too large (i.e. with a small spherical variance) will result in an underrepresentation of the oval tails of the data. All these problems will result in an incorrect modelling of connectivity, that is positively correlated to orientation dispersion (e.g. Smith et al., 2013).

A possible workaround for this problem, using the available software, could be to split the oval clusters and fit multiple Fisher distributions to model their parts, possibly validating the results generating synthetic clusters and comparing them with the natural ones. More in general, more advanced distributions such as the, Kent, Bingham-5-parameters, Bingham-8-parameters or mixed Bingham can be adopted to fit asymmetrical or multimodal clusters (Kurz et al., 2014; Gilitschenski et al., 2016; Yamaji, 2016), and we feel that adopting at least the Kent distribution in stochastic modelling applications would be a significant improvement along the path of creating realistic stochastic fracture networks.

11.3 Topology

In the ongoing discussion on topological analysis in fracture studies, some authors (e.g. Sanderson and Nixon, 2015) proposed to consider the connectivity of fracture branches, instead of full fracture traces, due to a supposed uncertainty in unravelling crosscutting, abutting, or splay relationships when branches form a small angle. From an almost opposite perspective, other authors (Forstner and Laubach, 2022) suggest considering also contingent nodes (C nodes) that would allow merging individual small branches to form larger traces, based on genetic or hydraulic considerations. In this context, we like to recall that (i) linear traces or branches represent the intersection of fracture surfaces with the outcrop surface (e.g. Sanderson and Nixon, 2015), and that (ii) most of the time we are actually interested in fracture surfaces rather than in their traces. In other words, branch connectivity parameters and length distribution can be useful information to characterize 2D connectivity of lines, but we would like to stress that considering branch length data as if they were full trace lengths would dramatically underestimate the dimensions of the underlying fracture surfaces, overestimate fracture density (since branches are more numerous that full traces) and would not allow performing directional topology analysis on a per-set basis, as

https://doi.org/10.5194/egusphere-2025-1398
Preprint. Discussion started: 11 April 2025

discussed above. For these reasons we insist in considering fracture traces, relying on geological information collected in the field to solve the ambiguity highlighted by Sanderson and Nixon (2015).

Directional topology adds a further layer to the fracture network characterization by assigning every node to specific fracture set(s). This allows quantifying crosscutting and abutting relationships between different fracture sets and understanding how the different fracture sets contribute to the overall connectivity of the fracture network. At the same time, it is possible to derive parameters like FBI that express the relative chronology and stratabound relationships in a more quantitative way. The necessity of excluding censored fracture traces from the FBI calculation might result in either an overestimation of this index, in case the longest traces tend to have I-nodes, or an underestimation in case they tend to terminate with Y-nodes. Unfortunately, this effect is very difficult to assess at the moment, and we leave a more detailed analysis for future studies.

Extracting the backbone of the trace network as in Figure 9, i.e. the largest connected cluster of the network, seems a really interesting result, and is possible thanks to the code we developed (https://github.com/gecos-lab/FracAbility). However, we would like to raise some cautionary note about these results. In fact in our outcrop the backbone is located along one of the major structures present in the pavement but, at the same time, it has been detected in a zone of the pavement that is very clean and free from quarrying-induced fractures, and it is bound by zones where the possibility to detect smaller fractures belonging to Set 2 and 3 is more limited. Therefore, there is no way of knowing if the shape and position of the backbone are due only to the presence of a major structure, or if they would change if other areas of the outcrop were not disturbed. In conclusion, the backbone detected by our analysis probably represents a subset of what it could be, if a complete undisturbed dataset was available. This also means that the connectivity index of the whole fracture network is probably underestimated, even in such a high-quality outcrop.

11.4 Length and height distributions

Of the four major biases that hinder the definition of a correct length and height distribution, censoring is the only one that cannot be addressed by changing sampling strategy (as for size and orientation bias) or improving data acquisition techniques and checking the quality of the input data by quantifying the resolution of the TS-DOM with respect to the smallest fracture that can be detected (truncation bias, Section 7). This has led to excluding censored data (Bisdom et al., 2014) or considering censored fractures as complete ones (Panara et al., 2024; Smeraglia et al., 2021), resulting in statistical models that always underestimate length (Benedetti et al., 2024). At the same time, non-parametric approaches do not provide a fully specified parametric distribution (Mauldon et al., 2001), that is a fundamental input data in applications such as stochastic models, and also to evaluate the meaning of data in general (i.e. knowing the mean without any hint on standard deviation is meaningless). The censoring correction obtained by (Benedetti et al., 2024) with survival analysis allows to use the full extent of the dataset collected from TS-DOM, and obtaining an unbiased statistical distribution.

In this contribution we leverage the availability of both pavement and vertical wall exposures, obtaining an H/L ratio specific for our outcrop. This is a significant improvement with respect to previous approaches, where the H/L ratio is generally

https://doi.org/10.5194/egusphere-2025-1398
Preprint. Discussion started: 11 April 2025

assumed based e.g. on theoretical mechanical considerations, without any comparison with empirical data (Odling et al., 1999; Schultz and Fossen, 2002, and references therein).

The approach we propose, however, is not completely immune from a-priori assumptions. In fact, even in ideal outcrops, it is impossible to actually measure H/L of a single fracture surface because either we see the direct connection of the fracture surface in the vertical and pavement exposures – but in this case both traces are censored, or we see complete traces – but in this case we cannot see the connection. Our assumption is that height and length statistics must be correlated according to size rank, as discussed above in Section 9, and we believe that this is a reasonable assumption based e.g. on mechanical considerations (Odling et al., 1999) and results of our linear regression (Figure 15) but it is nevertheless important to state this transparently.

11.5 Fracture intensity and representative elementary area

Areal fracture intensity P_{21} is quite often calculated using scan areas of arbitrary size, without defining a proper representative sampling area (e.g. Bisdom et al., 2014; Menegoni et al., 2024; Panara et al., 2024). To our knowledge, only Martinelli et al. (2020) presented an analysis allowing to define the minimum REA where fracture intensity can be mediated to ensure a proper continuum-equivalent description (Bear, 1975).

As a partial correction to the approach in Martinelli et al. (2020), we recently noticed that the finite nature of outcrops determines limits in the collection of P_{21} data, such as the progressive decrease in scan areas numerosity as the scan area is increased, and the non-independence of P_{21} samples collected at increasing scan area sizes. For these reasons a step behind has been taken with respect to the application of formal statistical tests in the definition of REA (Martinelli et al., 2020), adopting a more qualitative approach which, however, does not require such stringent assumptions as the tests used by (Martinelli et al., 2020).

In any case we believe that, in addition to formal statistical reasons, defining the REA has very important practical applications. For instance, the choice of the optimal cell size in reservoir-scale models stems from a combination of several factors, that are the geological characteristics of the area, lithostratigraphic heterogeneities, mean spacing between wells and the available computational power. In general, however, there is a lower limit to the resolution of the model - around 50 m of cell size, dictated by computational power. This is an important piece of information because it outlines the minimum size that an analogue outcrop should have to capture all the variability within a hypothetical cell. From this point of view, the Pontrelli quarry provides a pavement two to three times larger than the minimum cell size, granting a sufficient area to calculate representative statistics. At the same time, the P_{21} REA, determined for Set 1 fractures between 5m and 12m, is approximately five to ten times smaller than the minimum cell size, allowing a safe application of continuum-equivalent upscaling techniques.

https://doi.org/10.5194/egusphere-2025-1398
Preprint. Discussion started: 11 April 2025

12 Conclusions

In this contribution, we presented a series of methods for measuring every relevant parameter to characterize a fracture network, particularly under the point of view of stochastic modelling approaches from well-exposed analogue outcrops. Our work shows that:

- Despite the high quality of the outcrop exposure at cava Pontrelli, not all parameters could be measured for every fracture set due to variable exposure conditions over the large areas.
- Estimating H/L was not possible without introducing some assumption, even for the best exposed set and in presence of both horizontal and vertical exposures. Therefore, we opted to make our assumption as transparent and possible, and testing it with regression analysis.
- All other parameters can be characterized based on robust statistical methodologies, which allow to evaluate the uncertainties associated to the measured fracture parameters.

From the case study point of view, the three tectonic related fracture set identified in Pontrelli quarry provide a complete view of what may or may not be obtained from an outcrop, depending on the conditions (vegetation, debris, quarrying activities) and the geometric relationships between the fractures and the outcrop planes. Parameters that cannot be calculated should be estimated (if possible) introducing geologically based assumptions that must be made explicit. To summarize these results:

- Set 1 represents the highest standard in terms of geometric properties that can be obtained from an outcrop. Fracture traces are homogeneously distributed across the pavement, and the perpendicular relationships between the fracture set and the outcrop vertical wall allows the collection of a meaningful statistical sample of both traces and facets.
- Set 2 still provides a complete set of data from the pavement and the wall (even if with a more limited statistical sample), but the sampling bias introduced by quarrying activities interfere with the correct estimation of the REA and the P_{21}.
- Set 3 is affected by the orientation bias on the vertical wall, therefor it is not possible to measure height and calculate the H/L ratio.
- While parameters of Set 1 have been almost completely characterized, we want to highlight that the analysis of statistical distributions of Set 2 and 3 is affected by slightly different biases and cannot be fully completed. This means that in case we need to model these sets with some stochastic approach, more assumptions must be made for the younger sets.

https://doi.org/10.5194/egusphere-2025-1398
Preprint. Discussion started: 11 April 2025

13 Code and data availability

Codes and data are available at the following GitHub repositories owned by the Gecos-lab group of the University of Milano – Bicocca (https://github.com/gecos-lab):

- FracAttitude: Python code for orientation data analysis available at https://github.com/gecos-lab/FracAttitude;
- DomStudioOrientation: Matlab code for orientation data analysis available at https://github.com/gecos-lab/DomStudioOrientation;
- FracAbility: Python toolbox for topology and survival analysis available at https://github.com/gecos-lab/FracAbility;
- FracAspect: Python code for H/L ratio calculation available at https://github.com/gecos-lab/FracAspect;
- FracElementary: Python code for P_{21} and REA analysis available at https://github.com/gecos-lab/FracElementary.

14 Author contribution

Andrea Bistacchi, Federico Agliardi and Bruno Monopoli conceived the first version of the orientation analysis workflow. Stefano Casiraghi, Andrea Bistacchi, Gabriele Benedetti, Silvia Mittempergher, Federico Agliardi and Daniela Bertacchi formulated the key concept of the paper and the final workflow structure. Fabio La Valle, Mattia Martinelli, Francesco Bigoni and Cristian Albertini participated to fundamental discussion throughout the project. Andrea Bistacchi and Stefano Casiraghi collected the raw photogrammetric data. Stefano Casiraghi performed DOM interpretation to generate the dataset. Stefano Casiraghi wrote the manuscript. Andrea Bistacchi, Silvia Mittempergher and Federico Agliardi heavily contributed in the revision process and in defining the final structure of the paper. Andrea Bistacchi lead the project and provided funding.

15 Competing interests

The authors declare that there are no competing interests.

16 Acknowledgements

We thank Eni SpA for funding, reviewing and agreeing to publish the results of the study. We thank SABAP – BA (Soprintendenza Archeologia, Belle Arti e Paesaggio per la Città Metropolitana di Bari) for granting the access to the Pontrelli quarry, making this work possible. We also thank François Bonneau for the fruitful discussions, in particular regarding directional topology.

https://doi.org/10.5194/egusphere-2025-1398
Preprint. Discussion started: 11 April 2025

17 References

Ackermann, R. V. and Schlische, R. W.: Anticlustering of small normal faults around larger faults, Geology, 25, 1127–1130, https://doi.org/10.1130/0091-7613(1997)025<1127:AOSNFA>2.3.CO;2, 1997.

Agliardi, F., Crosta, G. B., Meloni, F., Valle, C., and Rivolta, C.: Structurally-controlled instability, damage and slope failure in a porphyry rock mass, Tectonophysics, 605, 34–47, https://doi.org/10.1016/j.tecto.2013.05.033, 2013.

Agliardi, F., Zanchetta, S., and Crosta, G. B.: Fabric controls on the brittle failure of folded gneiss and schist, Tectonophysics, 637, 150–162, https://doi.org/10.1016/j.tecto.2014.10.006, 2014.

Agliardi, F., Dobbs, M. R., Zanchetta, S., and Vinciguerra, S.: Folded fabric tunes rock deformation and failure mode in the upper crust, Sci. Rep., 7, 15290, https://doi.org/10.1038/s41598-017-15523-1, 2017.

Akaike, H.: A new look at the statistical model identification, IEEE Trans. Autom. Control, 19, 716–723, https://doi.org/10.1109/TAC.1974.1100705, 1974.

Baecher, G. B.: Statistical analysis of rock mass fracturing, J. Int. Assoc. Math. Geol., 15, 329–348, https://doi.org/10.1007/BF01036074, 1983.

Baecher, G. B. and Lanney, N. A.: Trace Length Biases In Joint Surveys, 19th U.S. Symposium on Rock Mechanics (USRMS), 1978.

Barton, C. C., Hsieh, P. A., Angelier, J., Bergerat, F., Bouroz, C., Dettinger, M. D., and Weeks, E. P.: Physical and Hydrologic-Flow Properties of Fractures Las Vegas, Nevada—Zion Canyon, Utah—Grand Canyon, Arizona—Yucca Mountain, Nevada July 20–24, 1989, American Geophysical Union, Washington, D. C., https://doi.org/10.1029/FT385, 1989.

Bear, J.: Dynamics of Fluids in Porous Media, Soil Sci., 120, 162, https://doi.org/10.1097/00010694-19750800000022, 1975.

Bellian, J. A., Kerans, C., and Jennette, D. C.: Digital Outcrop Models: Applications of Terrestrial Scanning Lidar Technology in Stratigraphic Modeling, J. Sediment. Res., 75, 166–176, https://doi.org/10.2110/jsr.2005.013, 2005.

Benedetti, G., Casiraghi, S., Bertacchi, D., and Bistacchi, A. L. P.: Unbiased statistical length analysis of linear features: Adapting survival analysis to geological applications, https://doi.org/10.5194/egusphere-2024-2818, 30 September 2024.

Benedetti, G., Casiraghi, S., Bertacchi, D., and Bistacchi, A. L. P.: Unbiased statistical length analysis of linear features: Adapting survival analysis to geological applications, https://doi.org/10.5194/egusphere-2024-2818, 2025.

Bertrand, L., Géraud, Y., Le Garzic, E., Place, J., Diraison, M., Walter, B., and Haffen, S.: A multiscale analysis of a fracture pattern in granite: A case study of the Tamariu granite, Catalunya, Spain, J. Struct. Geol., 78, 52–66, https://doi.org/10.1016/j.jsg.2015.05.013, 2015.

Bisdom, K., Gauthier, B. D. M., Bertotti, G., and Hardebol, N. J.: Calibrating discrete fracture-network models with a carbonate three-dimensional outcrop fracture network: Implications for naturally fractured reservoir modeling, AAPG Bull., 98, 1351–1376, https://doi.org/10.1306/02031413060, 2014.

Bistacchi, A., Balsamo, F., Storti, F., Mozafari, M., Swennen, R., Solum, J., Tueckmantel, C., and Taberner, C.: Photogrammetric digital outcrop reconstruction, visualization with textured surfaces, and three-dimensional structural

https://doi.org/10.5194/egusphere-2025-1398
Preprint. Discussion started: 11 April 2025

analysis and modeling: Innovative methodologies applied to fault-related dolomitization (Vajont Limestone, Southern Alps, Italy), Geosphere, 11, 2031–2048, https://doi.org/10.1130/GES01005.1, 2015.

Bistacchi, A., Mittempergher, S., Martinelli, M., and Storti, F.: On a new robust workflow for the statistical and spatial analysis of fracture data collected with scanlines (or the importance of stationarity), Solid Earth, 11, 2535–2547, https://doi.org/10.5194/se-11-2535-2020, 2020.

Bistacchi, A., Massironi, M., and Viseur, S. (Eds.): 3D Digital Geological Models: From Terrestrial Outcrops to Planetary Surfaces, 1st ed., Wiley, https://doi.org/10.1002/9781119313922, 2022a.

Bistacchi, A., Mittempergher, S., and Martinelli, M.: Digital Outcrop Model Reconstruction and Interpretation, in: 3D Digital Geological Models, edited by: Bistacchi, A., Massironi, M., and Viseur, S., Wiley, 11–32, https://doi.org/10.1002/9781119313922.ch2, 2022b.

Bonneau, F., Henrion, V., Caumon, G., Renard, P., and Sausse, J.: A methodology for pseudo-genetic stochastic modeling of discrete fracture networks, Comput. Geosci., 56, 12–22, https://doi.org/10.1016/j.cageo.2013.02.004, 2013.

Bonneau, F., Caumon, G., and Renard, P.: Impact of a stochastic sequential initiation of fractures on the spatial correlations and connectivity of discrete fracture networks, J. Geophys. Res. Solid Earth, 121, 5641–5658, https://doi.org/10.1002/2015JB012451, 2016.

Boro, H., Rosero, E., and Bertotti, G.: Fracture-network analysis of the Latemar Platform (northern Italy): integrating outcrop studies to constrain the hydraulic properties of fractures in reservoir models, Pet. Geosci., 20, 79–92, https://doi.org/10.1144/petgeo2013-007, 2014.

Borradaile, G.: Statistics of Earth Science Data, Springer Berlin Heidelberg, Berlin, Heidelberg, https://doi.org/10.1007/978-3-662-05223-5, 2003.

Burnham, K. P. and Anderson, D. R.: Multimodel Inference: Understanding AIC and BIC in Model Selection, Sociol. Methods Res., 33, 261–304, https://doi.org/10.1177/0049124104268644, 2004.

Cox, S. F.: Injection-Driven Swarm Seismicity and Permeability Enhancement: Implications for the Dynamics of Hydrothermal Ore Systems in High Fluid-Flux, Overpressured Faulting Regimes—An Invited Paper, Econ. Geol., 111, 559–587, https://doi.org/10.2113/econgeo.111.3.559, 2016.

Davis, G. H., Reynolds, S. J., and Kluth, C.: Structural geology of rocks and regions, 3rd ed., John Wiley & Sons, Hoboken, 864 pp., 2012.

Davis, J. C.: Statistics and Data Analysis in Geology, 3rd ed., John Wiley & Sons, 2002.

Davy, P., Le Goc, R., and Darcel, C.: A model of fracture nucleation, growth and arrest, and consequences for fracture density and scaling, J. Geophys. Res. Solid Earth, 118, 1393–1407, https://doi.org/10.1002/jgrb.50120, 2013.

Dershowitz, W. S. and Einstein, H. H.: Characterizing rock joint geometry with joint system models, Rock Mech. Rock Eng., 21, 21–51, https://doi.org/10.1007/BF01019674, 1988.

Dershowitz, W. S. and Herda, H. H.: Interpretation of fracture spacing and intensity, The 33rd U.S. Symposium on Rock Mechanics (USRMS), ARMA-92-0757, 1992.

https://doi.org/10.5194/egusphere-2025-1398
Preprint. Discussion started: 11 April 2025

Dewez, T. J. B., Girardeau-Montaut, D., Allanic, C., and Rohmer, J.: FACETS : A CLOUDCOMPARE PLUGIN TO EXTRACT GEOLOGICAL PLANES FROM UNSTRUCTURED 3D POINT CLOUDS, Int. Arch. Photogramm. Remote Sens. Spat. Inf. Sci., XLI-B5, 799–804, https://doi.org/10.5194/isprs-archives-XLI-B5-799-2016, 2016.

Eberhardt, E., Stead, D., and Coggan, J. S.: Numerical analysis of initiation and progressive failure in natural rock slopes—the 1991 Randa rockslide, Int. J. Rock Mech. Min. Sci., 41, 69–87, https://doi.org/10.1016/S1365-1609(03)00076-5, 2004.

Fisher, N. I. and Best, D. J.: GOODNESS-OF-FIT TESTS FOR FISHER'S DISTRIBUTION ON THE SPHERE, Aust. J. Stat., 26, 142–150, https://doi.org/10.1111/j.1467-842X.1984.tb01228.x, 1984.

Fisher, R.: Dispersion on a sphere, Proc. R. Soc. Lond., 217, 295–305, 1953.

Fisher, R. A.: Statistical Methods for Research Workers, in: Breakthroughs in Statistics: Methodology and Distribution, edited by: Kotz, S. and Johnson, N. L., Springer, New York, NY, 66–70, https://doi.org/10.1007/978-1-4612-4380-9_6, 1992.

Follin, S., Hartley, L., Rhén, I., Jackson, P., Joyce, S., Roberts, D., and Swift, B.: A methodology to constrain the parameters of a hydrogeological discrete fracture network model for sparsely fractured crystalline rock, exemplified by data from the proposed high-level nuclear waste repository site at Forsmark, Sweden, Hydrogeol. J., 22, 313–331, https://doi.org/10.1007/s10040-013-1080-2, 2014.

Forstner, S. R. and Laubach, S. E.: Scale-dependent fracture networks, J. Struct. Geol., 165, 104748, https://doi.org/10.1016/j.jsg.2022.104748, 2022.

Franzosi, F., Casiraghi, S., Colombo, R., Crippa, C., and Agliardi, F.: Quantitative Evaluation of the Fracturing State of Crystalline Rocks Using Infrared Thermography, Rock Mech. Rock Eng., 56, 6337–6355, https://doi.org/10.1007/s00603-023-03389-x, 2023a.

Franzosi, F., Crippa, C., Derron, M.-H., Jaboyedoff, M., and Agliardi, F.: Slope-Scale Remote Mapping of Rock Mass Fracturing by Modeling Cooling Trends Derived from Infrared Thermography, Remote Sens., 15, 4525, https://doi.org/10.3390/rs15184525, 2023b.

Genter, A., Evans, K., Cuenot, N., Fritsch, D., and Sanjuan, B.: Contribution of the exploration of deep crystalline fractured reservoir of Soultz to the knowledge of enhanced geothermal systems (EGS), Comptes Rendus Geosci., 342, 502–516, https://doi.org/10.1016/j.crte.2010.01.006, 2010.

Gigli, G. and Casagli, N.: Semi-automatic extraction of rock mass structural data from high resolution LIDAR point clouds, Int. J. Rock Mech. Min. Sci., 48, 187–198, https://doi.org/10.1016/j.ijrmms.2010.11.009, 2011.

Gilitschenski, I., Kurz, G., Julier, S. J., and Hanebeck, U. D.: Unscented Orientation Estimation Based on the Bingham Distribution, IEEE Trans. Autom. Control, 61, 172–177, https://doi.org/10.1109/TAC.2015.2423831, 2016.

Giuffrida, A., Agosta, F., Rustichelli, A., Panza, E., La Bruna, V., Eriksson, M., Torrieri, S., and Giorgioni, M.: Fracture stratigraphy and DFN modelling of tight carbonates, the case study of the Lower Cretaceous carbonates exposed at the Monte Alpi (Basilicata, Italy), Mar. Pet. Geol., 112, 104045, https://doi.org/10.1016/j.marpetgeo.2019.104045, 2020.

Gleeson, T. and Ingebritsen, S. E.: Toward systematic characterization, in: Crustal Permeability, John Wiley & Sons, Ltd, 393–397, https://doi.org/10.1002/9781119166573.ch30, 2012.

https://doi.org/10.5194/egusphere-2025-1398
Preprint. Discussion started: 11 April 2025

Hadgu, T., Karra, S., Kalinina, E., Makedonska, N., Hyman, J. D., Klise, K., Viswanathan, H. S., and Wang, Y.: A comparative study of discrete fracture network and equivalent continuum models for simulating flow and transport in the far field of a hypothetical nuclear waste repository in crystalline host rock, J. Hydrol., 553, 59–70, https://doi.org/10.1016/j.jhydrol.2017.07.046, 2017.

Hancock, P. L.: Brittle microtectonics: principles and practice, J. Struct. Geol., 7, 437–457, https://doi.org/10.1016/0191-8141(85)90048-3, 1985.

Haridy, M. G., Sedighi, F., Ghahri, P., Ussenova, K., and Zhiyenkulov, M.: Comprehensive Study of the Oda Corrected Permeability Upscaling Method, in: Day 2 Wed, October 30, 2019, SPE/IATMI Asia Pacific Oil & Gas Conference and Exhibition, Bali, Indonesia, D022S006R006, https://doi.org/10.2118/196399-MS, 2020.

Healy, D., Rizzo, R. E., Cornwell, D. G., Farrell, N. J. C., Watkins, H., Timms, N. E., Gomez-Rivas, E., and Smith, M.: FracPaQ: A MATLAB™ toolbox for the quantification of fracture patterns, J. Struct. Geol., 95, 1–16, https://doi.org/10.1016/j.jsg.2016.12.003, 2017.

Hodgetts, D.: Laser scanning and digital outcrop geology in the petroleum industry: A review, Mar. Pet. Geol., 46, 335–354, https://doi.org/10.1016/j.marpetgeo.2013.02.014, 2013.

Immenhauser, A., Hillgärtner, H., Sattler, U., Bertotti, G., Schoepfer, P., Homewood, P., Vahrenkamp, V., Steuber, T., Masse, J.-P., Droste, H., Koppen, J. T., Van Der Kooij, B., Van Bentum, E., Verwer, K., Strating, E. H., Swinkels, W., Peters, J., Immenhauser-Potthast, I., and Al Maskery, S.: Barremian-lower Aptian Qishn Formation, Haushi-Huqf area, Oman: a new outcrop analogue for the Kharaib/Shu'aiba reservoirs, GeoArabia, 9, 153–194, https://doi.org/10.2113/geoarabia0901153, 2004.

Jacquemyn, C., Huysmans, M., Hunt, D., Casini, G., and Swennen, R.: Multi-scale three-dimensional distribution of fracture- and igneous intrusion- controlled hydrothermal dolomite from digital outcrop model, Latemar platform, Dolomites, northern Italy, AAPG Bull., 99, 957–984, https://doi.org/10.1306/10231414089, 2015.

Kaplan, E. L. and Meier, P.: Nonparametric Estimation from Incomplete Observations, J. Am. Stat. Assoc., 53, 457–481, https://doi.org/10.1080/01621459.1958.10501452, 1958.

Karvounis, D. and Wiemer, S.: A discrete fracture hybrid model for forecasting diffusion-induced seismicity and power generation in enhanced geothermal systems, Geophys. J. Int., 230, 84–113, https://doi.org/10.1093/gji/ggac056, 2022.

Kaufman, L. and Rousseeuw, P. J.: Clustering by means of medoids, Stat. Data Anal. Based L1 Norm Relat. Methods, 405–416, 1987.

Kaufman, L. and Rousseeuw, P. J.: Finding groups in data: an introduction to cluster analysis, Wiley, Hoboken, N.J, 342 pp., 2005.

Kent, J. T.: The Fisher-Bingham Distribution on the Sphere, J. R. Stat. Soc. Ser. B Methodol., 44, 71–80, https://doi.org/10.1111/j.2517-6161.1982.tb01189.x, 1982.

Kim, N.: Tests based on EDF statistics for randomly censored normal distributions when parameters are unknown, Commun. Stat. Appl. Methods, 26, 431–443, https://doi.org/10.29220/CSAM.2019.26.5.431, 2019.

Kosović, I., Matoš, B., University of Zagreb, Faculty of Mining, Geology and Petroleum Engineering, Zagreb, Croatia, Casiraghi, S., Benedetti, G., Frangen, T., Urumović, K., Pavičić, I., Bistacchi, A., Mittempergher, S., Pola, M., and Borović,

https://doi.org/10.5194/egusphere-2025-1398
Preprint. Discussion started: 11 April 2025

S.: Hydrogeological parameterisation of the Daruvar thermal aquifer: integration of fracture network analysis and well testing, Geol. Croat., 77, 99–125, https://doi.org/10.4154/gc.2024.11, 2024.

Kulatilake, P. H. S. W. and Wu, T. H.: Estimation of mean trace length of discontinuities, Rock Mech. Rock Eng., 17, 215–232, https://doi.org/10.1007/BF01032335, 1984.

Kurz, G., Gilitschenski, I., Julier, S., and Hanebeck, U. D.: Recursive Bingham Filter for Directional Estimation Involving 180 Degree Symmetry, J. Adv. Inf. FUSION, VOL. 9, 2014.

Laubach, S. E., Lander, R. H., Criscenti, L. J., Anovitz, L. M., Urai, J. L., Pollyea, R. M., Hooker, J. N., Narr, W., Evans, M. A., Kerisit, S. N., Olson, J. E., Dewers, T., Fisher, D., Bodnar, R., Evans, B., Dove, P., Bonnell, L. M., Marder, M. P., and Pyrak-Nolte, L.: The Role of Chemistry in Fracture Pattern Development and Opportunities to Advance Interpretations of Geological Materials, Rev. Geophys., 57, 1065–1111, https://doi.org/10.1029/2019RG000671, 2019.

Lawless, J. F.: Statistical Models and Methods for Lifetime Data, John Wiley & Sons, 662 pp., 2011.

Leung, K.-M., Elashoff, R. M., and Afifi, A. A.: Censoring Issues in Survival Analysis, Annu. Rev. Public Health, 18, 83–104, https://doi.org/10.1146/annurev.publhealth.18.1.83, 1997.

Lewis, T. and Fisher, N. I.: Graphical methods for investigating the fit of a Fisher distribution to spherical data, Geophys. J. Int., 69, 1–13, https://doi.org/10.1111/j.1365-246X.1982.tb04931.x, 1982.

Mandl, G.: Rock Joints, Springer-Verlag, Berlin/Heidelberg, https://doi.org/10.1007/b137623, 2005.

Manzocchi, T.: The connectivity of two-dimensional networks of spatially correlated fractures, Water Resour. Res., 38, 1-1-1–20, https://doi.org/10.1029/2000WR000180, 2002.

March, R., Elder, H., Doster, F., and Geiger, S.: Accurate Dual-Porosity Modeling of CO2 Storage in Fractured Reservoirs, in: Day 3 Wed, February 22, 2017, SPE Reservoir Simulation Conference, Montgomery, Texas, USA, D031S012R004, https://doi.org/10.2118/182646-MS, 2017.

March, R., Doster, F., and Geiger, S.: Assessment of CO_2 Storage Potential in Naturally Fractured Reservoirs With Dual-Porosity Models, Water Resour. Res., 54, 1650–1668, https://doi.org/10.1002/2017WR022159, 2018.

Mardia, K. V. and Jupp, P. E.: Directional statistics, J. Wiley, Chichester ; New York, 429 pp., 2000.

Martinelli, M., Bistacchi, A., Mittempergher, S., Bonneau, F., Balsamo, F., Caumon, G., and Meda, M.: Damage zone characterization combining scan-line and scan-area analysis on a km-scale Digital Outcrop Model: The Qala Fault (Gozo), J. Struct. Geol., 140, 104144, https://doi.org/10.1016/j.jsg.2020.104144, 2020.

Mauldon, M.: Estimating Mean Fracture Trace Length and Density from Observations in Convex Windows, Rock Mech. Rock Eng., 31, 201–216, https://doi.org/10.1007/s006030050021, 1998.

Mauldon, M., Dunne, W. M., and Rohrbaugh, M. B.: Circular scanlines and circular windows: new tools for characterizing the geometry of fracture traces, J. Struct. Geol., 23, 247–258, https://doi.org/10.1016/S0191-8141(00)00094-8, 2001.

Mccaffrey, K. J. W., Jones, R. R., Holdsworth, R. R. E., Wilson, R. R. W., Clegg, P., Imber, J., Holliman, N., and Trinks, I.: Unlocking the spatial dimension: digital technologies and the future of geoscience fieldwork, J. Geol. Soc., 162, 927–938, https://doi.org/10.1144/0016-764905-017, 2005.

https://doi.org/10.5194/egusphere-2025-1398
Preprint. Discussion started: 11 April 2025

Menegoni, N., Giordan, D., Perotti, C., and Tannant, D. D.: Detection and geometric characterization of rock mass discontinuities using a 3D high-resolution digital outcrop model generated from RPAS imagery – Ormea rock slope, Italy, Eng. Geol., 252, 145–163, https://doi.org/10.1016/j.enggeo.2019.02.028, 2019.

Menegoni, N., Panara, Y., Greenwood, A., Mariani, D., Zanetti, A., and Hetényi, G.: Fracture network characterisation of the Balmuccia peridotite using drone-based photogrammetry, implications for active-seismic site survey for scientific drilling, J. Rock Mech. Geotech. Eng., S1674775524001495, https://doi.org/10.1016/j.jrmge.2024.03.012, 2024.

Menéndez, J., Ordóñez, A., Álvarez, R., and Loredo, J.: Energy from closed mines: Underground energy storage and geothermal applications, Renew. Sustain. Energy Rev., 108, 498–512, https://doi.org/10.1016/j.rser.2019.04.007, 2019.

Micklethwaite, S.: Mechanisms of faulting and permeability enhancement during epithermal mineralisation: Cracow goldfield, Australia, J. Struct. Geol., 31, 288–300, https://doi.org/10.1016/j.jsg.2008.11.016, 2009.

Moder, K.: Alternatives to F-Test in One Way ANOVA in case of heterogeneity of variances (a simulation study), 2010.

Nicosia, U., Marino, M., Mariotti, N., Muraro, C., Panigutti, S., Petti, F. M., and Sacchi, E.: The Late Cretaceus dinosaur tracksite near Altamura (Bari, Southern Italy), Geol. Romana, 35, 237–247, 1999.

Nyberg, B., Nixon, C. W., and Sanderson, D. J.: NetworkGT: A GIS tool for geometric and topological analysis of two-dimensional fracture networks, Geosphere, 14, 1618–1634, https://doi.org/10.1130/GES01595.1, 2018.

Odling, N. E.: Scaling and connectivity of joint systems in sandstones from western Norway, J. Struct. Geol., 19, 1257–1271, https://doi.org/10.1016/S0191-8141(97)00041-2, 1997.

Odling, N. E., Gillespie, P., Bourgine, B., Castaing, C., Chiles, J.-P., Christensen, N. P., Fillion, E., Genter, A., Olsen, C., Thrane, L., Trice, R., Aarseth, E., Walsh, J. J., and Watterson, J.: Variations in fracture system geometry and their implications for fluid flow in fractured hydrocarbon reservoirs, Pet. Geosci., https://doi.org/10.1144/petgeo.5.4.373, 1999.

Ortega, O. J., Marrett, R. A., and Laubach, S. E.: A scale-independent approach to fracture intensity and average spacing measurement, AAPG Bull., 90, 193–208, https://doi.org/10.1306/08250505059, 2006.

Pahl, P. J.: Estimating the Mean Length of Discontinuity Traces, Int J Rock Mech Min Sci Geomech, 18, 221 to 228, 1981.

Panara, Y., Menegoni, N., Finkbeiner, T., Zühlke, R., and Vahrenkamp, V.: High-resolution analysis of 3D fracture networks from Digital Outcrop Models, correlation to plate-tectonic events and calibration of subsurface models (Jurassic, Arabian Plate), Mar. Pet. Geol., 167, 106998, https://doi.org/10.1016/j.marpetgeo.2024.106998, 2024.

Panza, E., Berto, C., Luzi, E., Agosta, F., Zambrano, M., Tondi, E., Prosser, G., Giorgioni, M., and Janiseck, J. M.: Structural architecture and Discrete Fracture Network modelling of layered fractured carbonates (Altamura Fm., Italy), Ital. J. Geosci., 134, 409–422, https://doi.org/10.3301/IJG.2014.28, 2015.

Panza, E., Agosta, F., Rustichelli, A., Zambrano, M., Tondi, E., Prosser, G., Giorgioni, M., and Janiseck, J. M.: Fracture stratigraphy and fluid flow properties of shallow-water, tight carbonates: The case study of the Murge Plateau (southern Italy), Mar. Pet. Geol., 73, 350–370, https://doi.org/10.1016/j.marpetgeo.2016.03.022, 2016.

Panza, E., Agosta, F., Rustichelli, A., Vinciguerra, S. C., Ougier-Simonin, A., Dobbs, M., and Prosser, G.: Meso-to-microscale fracture porosity in tight limestones, results of an integrated field and laboratory study, Mar. Pet. Geol., 103, 581–595, https://doi.org/10.1016/j.marpetgeo.2019.01.043, 2019.

https://doi.org/10.5194/egusphere-2025-1398
Preprint. Discussion started: 11 April 2025

Pringle, J. K., Howell, J. A., Hodgetts, D., Westerman, A. R., and Hodgson, D. M.: Virtual outcrop models of petroleum reservoir analogues: a review of the current state-of-the-art, First Break, 24, https://doi.org/10.3997/1365-2397.2006005, 2006.

Renshaw, C. E.: Influence of subcritical fracture growth on the connectivity of fracture networks, Water Resour. Res., 32, 1519–1530, https://doi.org/10.1029/96WR00711, 1996.

Riquelme, A. J., Abellán, A., Tomás, R., and Jaboyedoff, M.: A new approach for semi-automatic rock mass joints recognition from 3D point clouds, Comput. Geosci., 68, 38–52, https://doi.org/10.1016/j.cageo.2014.03.014, 2014.

Riquelme, A. J., Abellán, A., and Tomás, R.: Discontinuity spacing analysis in rock masses using 3D point clouds, Eng. Geol., 195, 185–195, https://doi.org/10.1016/j.enggeo.2015.06.009, 2015.

Riva, F., Agliardi, F., Amitrano, D., and Crosta, G. B.: Damage-Based Time-Dependent Modeling of Paraglacial to Postglacial Progressive Failure of Large Rock Slopes, J. Geophys. Res. Earth Surf., 123, 124–141, https://doi.org/10.1002/2017JF004423, 2018.

Rohrbaugh Jr., M. B., Dunne, W. M., and Mauldon, M.: Estimating fracture trace intensity, density, and mean length using circular scan lines and windows, AAPG Bull., 86, https://doi.org/10.1306/61EEDE0E-173E-11D7-8645000102C1865D, 2002.

Sanderson, D. J. and Nixon, C. W.: The use of topology in fracture network characterization, J. Struct. Geol., 72, 55–66, https://doi.org/10.1016/j.jsg.2015.01.005, 2015.

Sanderson, D. J., Peacock, D. C. P., Nixon, C. W., and Rotevatn, A.: Graph theory and the analysis of fracture networks, J. Struct. Geol., 125, 155–165, https://doi.org/10.1016/j.jsg.2018.04.011, 2019.

Schultz, D. R. A.: Geologic Fracture Mechanics, 2019.

Schultz, R. A. and Fossen, H.: Displacement–length scaling in three dimensions: the importance of aspect ratio and application to deformation bands, J. Struct. Geol., 24, 1389–1411, https://doi.org/10.1016/S0191-8141(01)00146-8, 2002.

Sethian, J. A.: Fast Marching Methods, SIAM Rev., 41, 199–235, https://doi.org/10.1137/S0036144598347059, 1999.

Shakiba, M., Lake, L. W., Gale, J. F. W., Laubach, S. E., and Pyrcz, M. J.: Stochastic reconstruction of fracture network pattern using spatial point processes, Geoenergy Sci. Eng., 236, 212741, https://doi.org/10.1016/j.geoen.2024.212741, 2024.

Smeraglia, L., Mercuri, M., Tavani, S., Pignalosa, A., Kettermann, M., Billi, A., and Carminati, E.: 3D Discrete Fracture Network (DFN) models of damage zone fluid corridors within a reservoir-scale normal fault in carbonates: Multiscale approach using field data and UAV imagery, Mar. Pet. Geol., 126, 104902, https://doi.org/10.1016/j.marpetgeo.2021.104902, 2021.

Smith, S. A. F., Bistacchi, A., Mitchell, T. M., Mittempergher, S., and Di Toro, G.: The structure of an exhumed intraplate seismogenic fault in crystalline basement, Tectonophysics, 599, 29–44, https://doi.org/10.1016/j.tecto.2013.03.031, 2013.

Stahle, L. and Wold, S.: Analysis of variance (ANOVA), Chemom. Intell. Lab. Syst., 6, 259–272, https://doi.org/10.1016/0169-7439(89)80095-4, 1989.

Staub, I., Fredriksson, A., and Outters, N.: Strategy for a Rock Mechanics Site Descriptive Model. Development and testing of the theoretical approach, 2002.

https://doi.org/10.5194/egusphere-2025-1398
Preprint. Discussion started: 11 April 2025

Stephens, M. A.: EDF Statistics for Goodness of Fit and Some Comparisons, J. Am. Stat. Assoc., 69, 730–737, https://doi.org/10.1080/01621459.1974.10480196, 1974.

Storti, F., Bistacchi, A., Borsani, A., Balsamo, F., Fetter, M., and Ogata, K.: Spatial and spacing distribution of joints at (over-) saturation in the turbidite sandstones of the Marnoso-Arenacea Fm. (Northern Apennines, Italy), J. Struct. Geol., 156, 104551, https://doi.org/10.1016/j.jsg.2022.104551, 2022.

Sturzenegger, M. and Stead, D.: Close-range terrestrial digital photogrammetry and terrestrial laser scanning for discontinuity characterization on rock cuts, Eng. Geol., 106, 163–182, https://doi.org/10.1016/j.enggeo.2009.03.004, 2009.

Sturzenegger, M., Stead, D., and Elmo, D.: Terrestrial remote sensing-based estimation of mean trace length, trace intensity and block size/shape, Eng. Geol., 119, 96–111, https://doi.org/10.1016/j.enggeo.2011.02.005, 2011.

Tavani, S., Granado, P., Corradetti, A., Girundo, M., Iannace, A., Arbués, P., Muñoz, J. A., and Mazzoli, S.: Building a virtual outcrop, extracting geological information from it, and sharing the results in Google Earth via OpenPlot and Photoscan: An example from the Khaviz Anticline (Iran), Comput. Geosci., 63, 44–53, https://doi.org/10.1016/j.cageo.2013.10.013, 2014.

Terzaghi, R. D.: Sources of Error in Joint Surveys, Géotechnique, 15, 287–304, https://doi.org/10.1680/geot.1965.15.3.287, 1965.

Thiele, S., Grose, L., and Micklethwaite, S.: Compass: A CloudCompare workflow for digital mapping and structural analysis, 5548, 2018.

Townend, J., Sutherland, R., Toy, V. G., Doan, M., Célérier, B., Massiot, C., Coussens, J., Jeppson, T., Janku-Capova, L., Remaud, L., Upton, P., Schmitt, D. R., Pezard, P., Williams, J., Allen, M. J., Baratin, L., Barth, N., Becroft, L., Boese, C. M., Boulton, C., Broderick, N., Carpenter, B., Chamberlain, C. J., Cooper, A., Coutts, A., Cox, S. C., Craw, L., Eccles, J. D., Faulkner, D., Grieve, J., Grochowski, J., Gulley, A., Hartog, A., Henry, G., Howarth, J., Jacobs, K., Kato, N., Keys, S., Kirilova, M., Kometani, Y., Langridge, R., Lin, W., Little, T., Lukacs, A., Mallyon, D., Mariani, E., Mathewson, L., Melosh, B., Menzies, C., Moore, J., Morales, L., Mori, H., Niemeijer, A., Nishikawa, O., Nitsch, O., Paris, J., Prior, D. J., Sauer, K., Savage, M. K., Schleicher, A., Shigematsu, N., Taylor-Offord, S., Teagle, D., Tobin, H., Valdez, R., Weaver, K., Wiersberg, T., and Zimmer, M.: Petrophysical, Geochemical, and Hydrological Evidence for Extensive Fracture-Mediated Fluid and Heat Transport in the Alpine Fault's Hanging-Wall Damage Zone, Geochem. Geophys. Geosystems, 18, 4709–4732, https://doi.org/10.1002/2017GC007202, 2017.

Tukey, J. W.: Exploratory Data Analysis, Addison-Wesley Publ. Co. Read., https://doi.org/10.1002/bimj.4710230408, 1977.

Twiss, R. J. and Moores, E. M.: Structural Geology (2nd Ed.), W. H. Freeman, 532 pp., 2006.

Wallace, R. L., Cai, Z., Zhang, H., Zhang, K., and Guo, C.: Utility-scale subsurface hydrogen storage: UK perspectives and technology, Int. J. Hydrog. Energy, 46, 25137–25159, https://doi.org/10.1016/j.ijhydene.2021.05.034, 2021.

Wang, Q., Narr, W., and Laubach, S. E.: Quantitative characterization of fracture spatial arrangement and intensity in a reservoir anticline using horizontal wellbore image logs and an outcrop analogue, Mar. Pet. Geol., 152, 106238, https://doi.org/10.1016/j.marpetgeo.2023.106238, 2023.

Warburton, P. M.: A stereological interpretation of joint trace data, Int. J. Rock Mech. Min. Sci. Geomech. Abstr., 17, 181–190, https://doi.org/10.1016/0148-9062(80)91084-0, 1980.

https://doi.org/10.5194/egusphere-2025-1398
Preprint. Discussion started: 11 April 2025

Warren, J. E. and Root, P. J.: The Behavior of Naturally Fractured Reservoirs, Soc. Pet. Eng. J., 3, 245–255, https://doi.org/10.2118/426-PA, 1963.

Yamaji A.: Genetic algorithm for fitting a mixed Bingham distribution to 3D orientations: a tool for the statistical and paleostress analyses of fracture orientations, Isl. Arc, 25, 72–83, https://doi.org/10.1111/iar.12135, 2016.

Zambrano, M., Tondi, E., Korneva, I., Panza, E., Agosta, F., Janiseck, J. M., and Giorgioni, M.: Fracture properties analysis and discrete fracture network modelling of faulted tight limestones, Murge Plateau, Italy, Ital. J. Geosci., 135, 55–67, https://doi.org/10.3301/IJG.2014.42, 2016.

Zamehrian, M. and Sedaee, B.: Underground hydrogen storage in a naturally fractured gas reservoir: The role of fracture, Int. J. Hydrog. Energy, 47, 39606–39618, https://doi.org/10.1016/j.ijhydene.2022.09.116, 2022.

Zhang, L. and Einstein, H. H.: Estimating the Mean Trace Length of Rock Discontinuities, Rock Mech. Rock Eng., 31, 217–235, https://doi.org/10.1007/s006030050022, 1998.

Zhang, L., Einstein, H. H., and Dershowitz, W. S.: Stereological relationship between trace length and size distribution of elliptical discontinuities, Géotechnique, 52, 419–433, https://doi.org/10.1680/geot.2002.52.6.419, 2002.